

Line Voltage Drop Calculation in Unbalanced and Distorted Distribution Systems

Sonia Leva, *Member*, IEEE, Adriano P. Morando, and Dario Zaninelli, *Senior Member*, IEEE

Abstract: The classical problem of three-phase voltage drop calculation, well established in the case of sinusoidal positive sequence system, is extended in the paper with regard to unbalanced and distorted power systems. The adoption of the Park theory permits the introduction of the imaginary power in the voltage drop expression. The imaginary power generalizes the role of the reactive power in the classical treatment and permits to quantifies in one term only the effects on the voltage drop due simultaneously to the load instantaneous stored energy and to the presence of harmonic, interharmonics and sequence components.

Examples are reported in order to testify, in the case of unbalances and distortions, the effectiveness of the proposed formulation.

Index Terms - voltage drop, Park transformation, imaginary power, distorted and unbalanced systems, harmonics and interharmonics

I. INTRODUCTION

The voltage drop is one of the most important quantities in the characterization of transmission and distribution electric power systems. In fact it represents in a certain way the indicator of the effectiveness of the connection between the loads and the generation centers. The voltage drop control is also an essential task both for the stability and the economy of the power system and its calculation, even with the introduction of simplified procedures and approximations, is fundamental for the power system analysis [1].

The voltage drop calculation, in case of ac sinusoidal systems, had rise with the phasor's algebra, then, it was extended from the single-phase case to the three-phase balanced systems. Afterwards, the formulation of the symmetrical component's theory, starting by Stokvis [2], posed the problem of an extension to unbalanced sinusoidal case. Nowadays, the presence of harmonics and interharmonics in power systems point out the need of a new formulation of voltage drop expression [3], that generalizes the former phasorial one but that, in same time, takes into the account the contributions (instantaneous and average) of harmonics, interharmonics and unbalances.

In fact, in the presence of unbalances or/and distortions the accuracy of the voltage drop calculation becomes more weighty because the introduction of some simplifying hypotheses can bring to neglect some disturbance's contributions and then to wrong results.

The effort of the present paper is to analyze the concept of the voltage drop in three-phase systems under distorted and unbalanced conditions. In order to write the analysis results with the same formalism as the one used for single-phase systems and take into account the simultaneous contributions of the harmonic, interharmonic and sequence components to the voltage drop, the Park transformation is considered. This leads to reconsider the imaginary Park power as an extension of the reactive power concept to the distorted, unbalanced systems also from the point of view of the voltage drop, and not only from that of the line losses. In this respect, the use of the Park quantities is almost mandatory requirement coming from the application of the imaginary power [4,5,6].

II. THEORETICAL BACKGROUND: THE SINGLE-PHASE SINUSOIDAL CASE

Let consider the following complex equation:

$$\bar{V}_m = \bar{V}_v + (R + j\omega L)\bar{I} = \bar{V}_v + (R + jX)\bar{I} = \bar{V}_v + \bar{Z} \cdot \bar{I} \quad (1)$$

which represents a short single-phase line under sinusoidal conditions (fig.1a). The corresponding phasorial diagram is shown in fig.1b. Taking into account the approximate formulation, by Taylor series expansion of Pitagora's theorem, the phasorial diagram leads to the following relationship for the relative voltage drop:

$$\Delta\bar{v} = \frac{V_m - V_v}{V_v} = \frac{\Delta V}{V_v} \quad (2)$$

In the phasorial diagram of fig.1 ΔV is represented by the magnitude of vector $\overline{OD} - \overline{OA}$ and V_v by the magnitude of \overline{OA} . Therefore it can be written as:

$$\Delta\bar{v} \stackrel{\text{Taylor Series}}{\cong} \frac{RP + XQ}{V_v^2} + \frac{1}{2} \frac{I^2 (X\cos\varphi - R\sin\varphi)^2}{V_v^2 + RP + XQ} = f(I, \varphi) \quad (3)$$

P and Q being the active and reactive powers respectively, flowing across the right side line terminals. This result can be extended to three-phase circuits in the symmetrical and balanced case: in these conditions, in fact, a single-phase

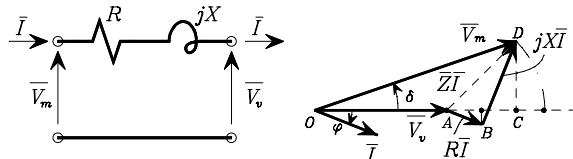


Fig.1. Short single-phase line. (a) Schematic. (b) Phasorial diagram

S. Leva is with the Electrical Engineering Department of the Politecnico di Milano, Milano, Italy (e-mail: sonia.leva@polimi.it)

A.P. Morando is with the Electrical Engineering Department of the Politecnico di Milano, Milano, Italy (e-mail: adriano.morando@polimi.it)

D. Zaninelli, is with the Electrical Engineering Department of the Politecnico di Milano, Milano, Italy (e-mail: dario.zaninelli@polimi.it)

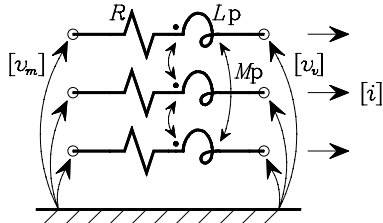


Fig. 2. Three-phase line with physical symmetry.

equivalent network can be employed to represent them. Usually, the function (3), in the case of inductive loads and small phase angle δ (fig.1b)², gives near the following value:

$$\Delta v \cong \frac{RP + XQ}{V_v^2} \quad (4)$$

Therefore the voltage drop results, in the sinusoidal case, a linear function of the active and reactive load powers. The meaning of (4) can be fully perceived by assigning a geometrical interpretation to the absolute voltage drop Δv . In fact, this scalar quantity can be considered as the projection of the phasor quantity $\bar{Z} \cdot \bar{I}$ in the direction oriented by the voltage phasor \bar{V}_v . It is indeed:

$$\Delta v = \underline{Z} \cdot \underline{I} \cdot \frac{\bar{V}_v}{V_v} = \Re e \left\{ \frac{\bar{Z} \cdot \bar{I} \cdot \bar{V}_v^*}{V_v} \right\} = \frac{RP + XQ}{V_v} \quad (5)$$

In this way the usually employed approximated formulation for the voltage drop is obtained. The employed approach can be immediately extended to three-phase circuits under non-sinusoidal conditions by applying the Fourier series decomposition and Park transformations.

III. THE PROPOSED METHOD: PARK APPROACH

In the most general case, the time-domain equations for a three-phase distribution line (see Fig.2) are differential equations. For the purposes of this work, they can be more clearly written in term of Heaviside operator [7,8] $p = d/dt$, so the line impedance vector z must be also written in terms of this operator as $z(p)$. Therefore, the time-domain equations for the line in Fig.1 can be written as:

$$[v_m(t)] = [v_v(t)] + [z(p)] \cdot [i(t)] \quad (6)$$

By applying the Park transformation³, the following relationships can be obtained:

$$\begin{cases} \bar{v}_m(t) = \bar{v}_v(t) + \bar{z}\bar{i}(t) + \ell p\bar{i}(t) \\ \bar{z} = R + j\hat{g}\ell = R + jX \\ L - M = \ell \end{cases} \quad (7)$$

² See appendix A.

³ See appendix B.

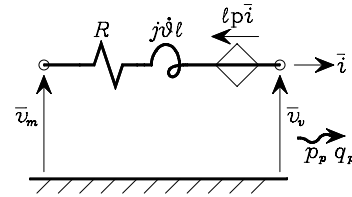


Fig. 3. Park representation of a two-port network representing a three-phase short line.

These equations are the Park equations describing the two-port network shown in Fig.3. They differ from those describing a single-phase line under sinusoidal conditions because of the presence of the dynamic term $\ell p\bar{i}(t)$.

It is known [5] that the application of the Park transformation allows for extending the phasor formalism adopted for the sinusoidal case to the non-sinusoidal one by substituting the instantaneous Park vectors to the phasor and the instantaneous rms value of the Park vector (Appendix A) to the sinusoidal quantities. Applying the rms instantaneous Park voltages, the relative voltage drop can be written as:

$$\Delta v(t) = \frac{|\bar{v}_m(t)| - |\bar{v}_v(t)|}{|\bar{v}_v(t)|} = \frac{v_m(t) - v_v(t)}{v_v(t)} \quad (8)$$

The formal extension of the geometrical approach typical of the sinusoidal case in three-phase systems leads - for small values of the phase angle δ (Fig.4) - to the following instantaneous rms voltage drop:

$$\begin{aligned} \Delta v(t) &= \frac{(\bar{z} + \ell p)\bar{i}(t) \cdot \bar{v}_v(t)}{v_v(t)} = \Re e \left\{ \bar{z} \cdot \bar{i}(t) \frac{\bar{v}_v^*(t)}{v_v^2(t)} + (\ell p\bar{i}(t)) \frac{\bar{v}_v^*(t)}{v_v^2(t)} \right\} = (9) \\ &= \frac{Rp_p(t) + Xq_p(t)}{v_v^2(t)} + \frac{\ell p p_p(t)}{v_v^2(t)} - \frac{\ell \bar{i}(t) \cdot p\bar{v}_v(t)}{v_v^2(t)} \end{aligned}$$

where $p_p(t) = \Re e\{\bar{v}_v(t) \cdot \bar{i}^*(t)\}$ is the instantaneous Park real power, and $q_p(t) = \Im m\{\bar{v}_v(t) \cdot \bar{i}^*(t)\}$ is the instantaneous Park imaginary power [4,5,6].

The following considerations apply to the expression (9).

- a) The first term represents the instantaneous voltage drop evaluated by means of an equation that is formally the same as for the single-phase case. Despite the similarity is once again formal, due to the fact that the instantaneous power $p_p(t)$ is considered instead of the active power P , and the instantaneous imaginary power $q_p(t)$ is considered instead of the reactive power Q , this term keeps its meaning extending it to the non-sinusoidal unbalanced condition. This extension is due to the presence of the

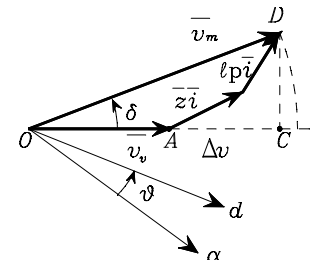


Fig. 4. Graphic representation of the drop voltage in the stationary $\alpha\beta$ plane and in the rotating dq one.

imaginary power, that is a dynamic term and is related not only to dielectric and magnetic phenomena but also to harmonic and sequence components [4,5,6,10].

- b) The second term is connected to the rate of variation of the load instantaneous power. This term gives further evidence that the optimal transmission is characterized by $p_p(t)=P=\text{constant}$ which is a specific condition of the balanced three-phase systems.
- c) The third term is related to the rate of variation of the voltage projected on the direction identified by the current Park vector. This term is nil when the stationary axes voltage Park vector describes a circumference with constant speed. This condition occurs when the supply voltages are sinusoidal and belong to the positive sequence only.

The approximation introduced by using (9) deduced by graphic approximations instead of (8) can be estimated and depends on the ratio between the line and load sequence inductance value, in a similar way as that indicated for the sinusoidal single-phase case, as shown in [9].

Equation (9) is valid under any condition. This gives to equation (9) the possibility to be applied to many systems condition, as for example the presence of static converters and non-linear loads.

IV. THE EFFECT OF HARMONIC AND SEQUENCE COMPONENTS ON THE VOLTAGE DROP UNDER NON-SINUSOIDAL CONDITIONS

On this line, the definition of the role performed by harmonics and sequence components present in the network becomes very important on the application point of view. Equation (9) can be reconsidered in order to clarify the dependence of $p_p(t)$, $q_p(t)$, $\bar{i}(t)$, $\bar{v}_v(t)$ on the harmonic and sequence components. Observing that [4,5]:

$$\left\{ \begin{array}{l} \bar{w}(t) = \sum_{h=-\infty}^{+\infty} \bar{w}_h(t) = \sum_{h=-\infty}^{+\infty} \bar{W}_h e^{j(h\omega - \theta)(t)} \\ \bar{a}_p(t) = \bar{v}(t) \cdot \bar{i}^*(t) = p_p(t) + jq_p(t) = \sum_{h=-\infty}^{+\infty} \bar{V}_h \bar{I}_h^* + \sum_{\substack{h=-\infty \\ h \neq k}}^{+\infty} \bar{V}_h \bar{I}_k^* e^{j(h-k)\omega t} \end{array} \right. \quad (10)$$

the different terms in (4) can be rewritten as:

$$\left\{ \begin{array}{l} \frac{Rp_p(t) + Xq_p(t)}{v_v^2(t)} = \left\{ R \cdot \Re e \left[\sum_{h=-\infty}^{+\infty} \bar{V}_h \bar{I}_h^* + \sum_{\substack{h=-\infty \\ h \neq k}}^{+\infty} \bar{V}_h \bar{I}_k^* e^{j(h-k)\omega t} \right] + \right. \\ \left. + X \cdot \Im m \left[\sum_{h=-\infty}^{+\infty} \bar{V}_h \bar{I}_h^* + \sum_{\substack{h=-\infty \\ h \neq k}}^{+\infty} \bar{V}_h \bar{I}_k^* e^{j(h-k)\omega t} \right] \right\} / \sum_{h=-\infty}^{+\infty} V_h^2 \\ \frac{\ell p p_p(t)}{v_v^2(t)} = \ell \cdot \Re e \left\{ \sum_{\substack{h=-\infty \\ h \neq k}}^{+\infty} (j(h-k)\omega) \bar{V}_h \bar{I}_k^* e^{j(h-k)\omega t} \right\} / \sum_{h=-\infty}^{+\infty} V_h^2 \\ \frac{\ell \bar{i}(t) \bullet p \bar{v}_v(t)}{v_v^2(t)} = \left\{ \ell \cdot \sum_{h=-\infty}^{+\infty} -(h\omega - \dot{\theta}) Q_h + \right. \\ \left. + \Re e \left\{ \sum_{\substack{h=-\infty \\ h \neq k}}^{+\infty} (-j \ell (k\omega - \dot{\theta})) \bar{V}_h \bar{I}_k^* e^{j(h-k)\omega t} \right\} \right\} / \sum_{k=-\infty}^{+\infty} V_h^2 \end{array} \right. \quad (11)$$

This result formally unifies the harmonic and sequence effects in three-phase circuits since it takes into account both the harmonic and sequence components as the components of the generalized Fourier series decomposition of the Park vector. In fact, each harmonic component k belongs to the positive sequence if $k>0$ or to the negative sequence if $k<0$ [5]. It presents the most general formulation of the voltage drop in physically symmetrical three-phase networks under non-sinusoidal condition. Moreover it confirms the presence of pulsating component on the voltage drop, giving evidence of the harmonic and sequence additional contribution with respect to the sinusoidal, positive sequence, balanced three-phase case.

A. Voltage drop average value and its connection with the classical expression

Starting from the above general expression of the voltage drop in time domain, it is possible to evaluate the following average value with reference to the interval $[t, t+T]$:

$$\langle \Delta v \rangle = \frac{1}{T} \int_t^{t+T} \Delta v(t) dt \quad (12)$$

This calculation is justified by the importance of the voltage rms value on the loads and distribution system operation. Applying (7) to the formula (6), it is possible to obtain:

$$\langle \Delta v \rangle = \frac{R \cdot \sum_{h=-\infty}^{+\infty} P_h + X \cdot \sum_{h=-\infty}^{+\infty} Q_h}{\sum_{h=-\infty}^{+\infty} V_h^2} - \frac{\ell \cdot \sum_{h=-\infty}^{+\infty} -(h\omega - \dot{\theta}) Q_h}{\sum_{k=-\infty}^{+\infty} V_h^2} \quad (13)$$

thus:

$$\langle \Delta v \rangle = \frac{R \cdot \sum_{h=-\infty}^{+\infty} P_h + \omega \ell \cdot \sum_{h=-\infty}^{+\infty} h Q_h}{\sum_{h=-\infty}^{+\infty} V_h^2} \quad (14)$$

The unbalanced sinusoidal case is of particular interest. In these conditions the presence of contributions associated to positive and negative sequences only brings to the following:

$$\langle \Delta v \rangle = \frac{R \cdot (P_1 + P_2) + \omega \ell \cdot (Q_1 - Q_2)}{V_1^2 + V_2^2} \quad (15)$$

In (10) it is possible to recognize a generalization of the classical expression typical of the presence of the positive sequence only.

In this case the reactive power – represented as maximum value in classical theory – appears as the average value of the imaginary power [4,5].

Referring P_h , Q_h and V_h present in (15) to the load representation shown in Fig.5, we obtain:

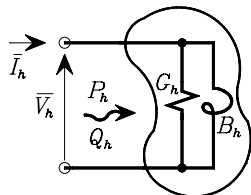


Fig.5. Load representation.

$$\begin{cases} V_h^2 = k_h V_1^2 \\ P_h = V_h^2 G_c \\ Q_h = V_h^2 B_c / h \end{cases} \quad (16)$$

And (9) becomes:

$$\langle \Delta v \rangle = \frac{RP_1 \cdot \sum_{h=-\infty}^{+\infty} k_h + \omega \ell Q_1 \cdot \sum_{h=-\infty}^{+\infty} k_h}{V_1^2 \cdot \sum_{h=-\infty}^{+\infty} k_h} = \frac{RP_1 + \omega \ell Q_1}{V_1^2} \quad (17)$$

This result shows that the voltage drop calculated for the fundamental harmonic component only represents the generalized average value of the voltage drop expressed in (10).

The obtained results suggest in addition the following comments. Concerning the size of system components, the use of the classical expression:

$$\Delta V = \frac{RP + \omega \ell Q}{V_v} \quad (18)$$

is confirmed. The important role is, in this case, assumed by the reactive power associated to the fundamental harmonic positive sequence. As concerns the compensation and stability [12] problems – that rely to dynamic topics – the use of the formula (10) derived from the Park approach is more appropriated giving results on time domain. In this case the imaginary power $q_p(t)$ takes the role of the reactive power Q .

V. THE EFFECT OF INTERHARMONIC COMPONENTS ON THE VOLTAGE DROP

It is particularly interesting the case in which interharmonics are present in the power system. In this case the general formulations (11,13,14) are still valid. Also the equations developed concerning the periodic conditions are valid when frequency, harmonic order and time period are referred to the basic quantities (i.e. the ones associated to the basic frequency of the correspondent waveform) instead of the network frequency (50 or 60 Hz).

In this case the Park quantities become:

$$\begin{cases} \overline{w}(t) = \sum_{h_F=-\infty}^{+\infty} \overline{w}_{h_F}(t) = \sum_{h_F=-\infty}^{+\infty} \overline{W}_{h_F} e^{j(h_F \omega_F t - \theta(t))} \\ \omega_F = \frac{2\pi}{T_F} = 2\pi f_F \end{cases} \quad (14)$$

where:

- f_F is the Fourier's basic frequency (it is the greatest common divisor of all the frequencies components in the signal);
- h_F is the harmonic order referred to f_F ;
- T_F is the period associated to the basic frequency.

Furthermore the relation between these latter quantities and the ones related to the network frequency:

$$\frac{h_F}{h} = \frac{f_F}{f} = \frac{T}{T_F} \quad (15)$$

VI SOME EXAMPLES

Some typical examples are here considered that refer to a short line supplying a passive load. The different examples differ for the voltage and current waveforms imposed at the output port.

In particular, the following situations are considered.

- The voltages imposed at the line output port are sinusoidal and belong to the positive sequence; the load draws sinusoidal currents of both positive and negative sequence ($I_2 = 0.25 \cdot I_1$). The voltages at the line-input port are obtained by means of (7). The considered circuit is shown in Fig.6a.
- The voltages imposed at the line output port are 6-step voltages with basic frequency 50Hz. The current drawn by the passive load is consequently unbalanced and distorted. The voltages at the line-input port are obtained by means of (7). The considered circuit is shown in Fig.7a.
- The voltages imposed at the line output port are periodical with subharmonic ($f_s=20\text{Hz}$, $V_s=0.1\text{V}$) and interharmonic ($f_i=320\text{Hz}$, $V_s=0.2\text{V}$) components, the basic component have $f=50\text{ Hz}$ with magnitude V . The current drawn by the passive load is consequently unbalanced and distorted. The voltages at the line-input port are obtained by means of (7). The considered circuit is shown in Fig.8a.

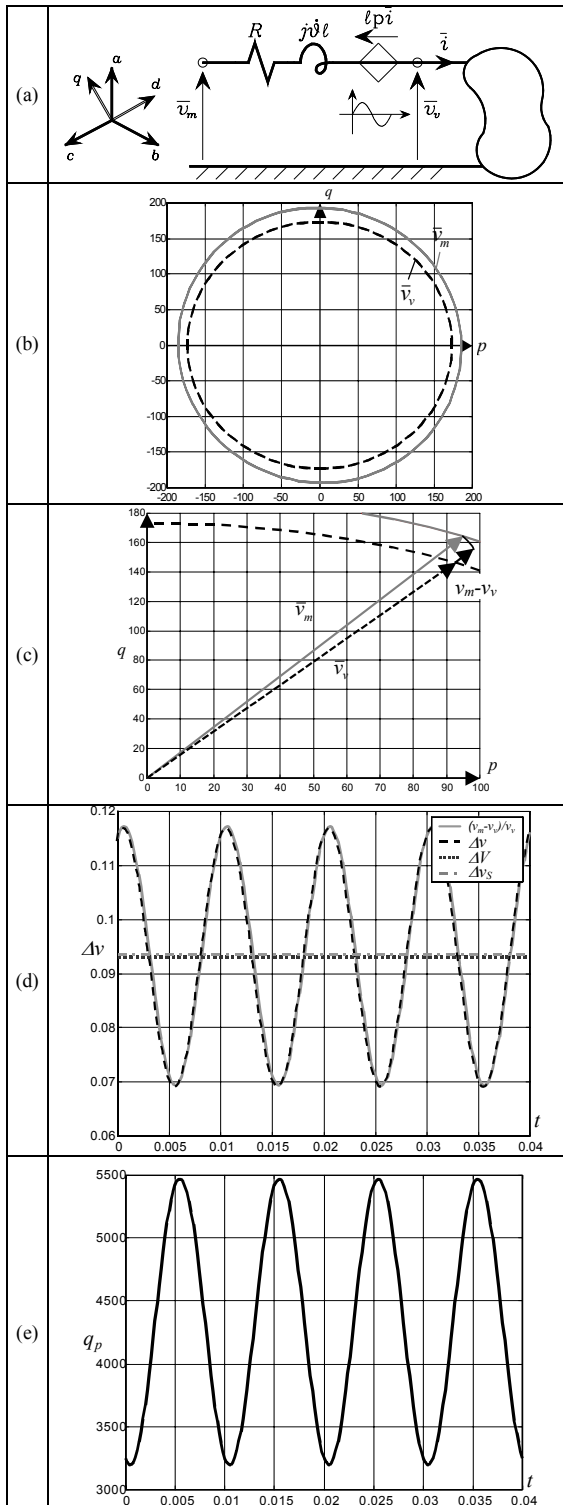


Fig.6. Numerical example where the voltages at the line output port are sinusoidal and belong to the positive sequence. (a) Circuit representation. (b) Polar diagram of Park voltages. \vec{v}_v : Dashed line; \vec{v}_m : solid line. (c) Enlargement of a significant portion of (b) diagram. (d) Voltage drop waveform given by (8), (9), (18) and by the symmetrical components theory. (e) Park imaginary power waveform

The following diagrams show the results of the above numerical simulation.

- Figures 6b, 7b and 8b show the polar diagrams of the Park vectors of the voltages at the input and output ports of the line. Figures 6c, 7c and 8c show the enlargements of a significant portion of the above diagrams, which stress the instantaneous voltage drop evaluated by (7) specifically expressed in terms of Park variables.
- Figures 6d, 7d and 8d show the voltage drop waveforms evaluated by means of the usual definition (8), the proposed relationship (9) and the classical formulation (18).
- Figures 6e, 7e and 8e show the Park imaginary power waveform.

The above mentioned diagrams show that:

- 1) The polar diagrams can be seen as an extension, in the $\{d, q, 0\}$ domain, of the phasorial diagrams typical of the sinusoidal single-phase conditions. They give evidence of the voltage drop in three-phase circuits in a much clearer way than the traditional approach, which works only under balanced symmetrical conditions.
- 2) The comparison of the diagrams in Figures 6d, 7d and 8d proves that the proposed algorithm, based on the Park approach, is correct, since the voltage drop diagram is the same as that computed using (8).
- 3) The exam of the diagrams in Figures 6d, 7d and 8d confirms the implication typical of classical theory: the classical voltage drop is equal to the mean value of the Park voltage drop.
- 4) The diagrams of the Park imaginary power show that this quantity has fairly the same waveform as the instantaneous voltage drop, and hence give evidence of the role of this quantity that is completely disregarded by the classical theory.

In the case of examples b) and c), that are studies referred to the harmonic distortion component (see Fig.7) and to the interharmonic ones (see Fig.8), respectively, a comparison is made with the results obtained by means of commercial software on power systems harmonics [13].

The simulation with this software brings to the point-dashed lines Δv_H in Figg.7d and 8d. These results represent the mean value of the voltage drop as seen by Park approach and then the classical voltage drop. This result put in evidence how the Park approach is the most general one. In fact, in addition to the general solution, the Park application can easily bring, through the evaluation of the mean value, to the classical voltage drop evaluation.

VII. CONCLUSIONS

The usual formulation of the voltage drop, generally limited to the sinusoidal balanced case, was extended to the most general non-sinusoidal unbalanced case. This extension gives evidence of the effects of the harmonic and sequence components. In particular, the analysis in terms of the Park vector confirms the single-phase nature of the Park variables and stresses the role of the Park imaginary power. This last quantity appears to be a generalization of the reactive power concept to any operating condition as far as the voltage drop is considered.

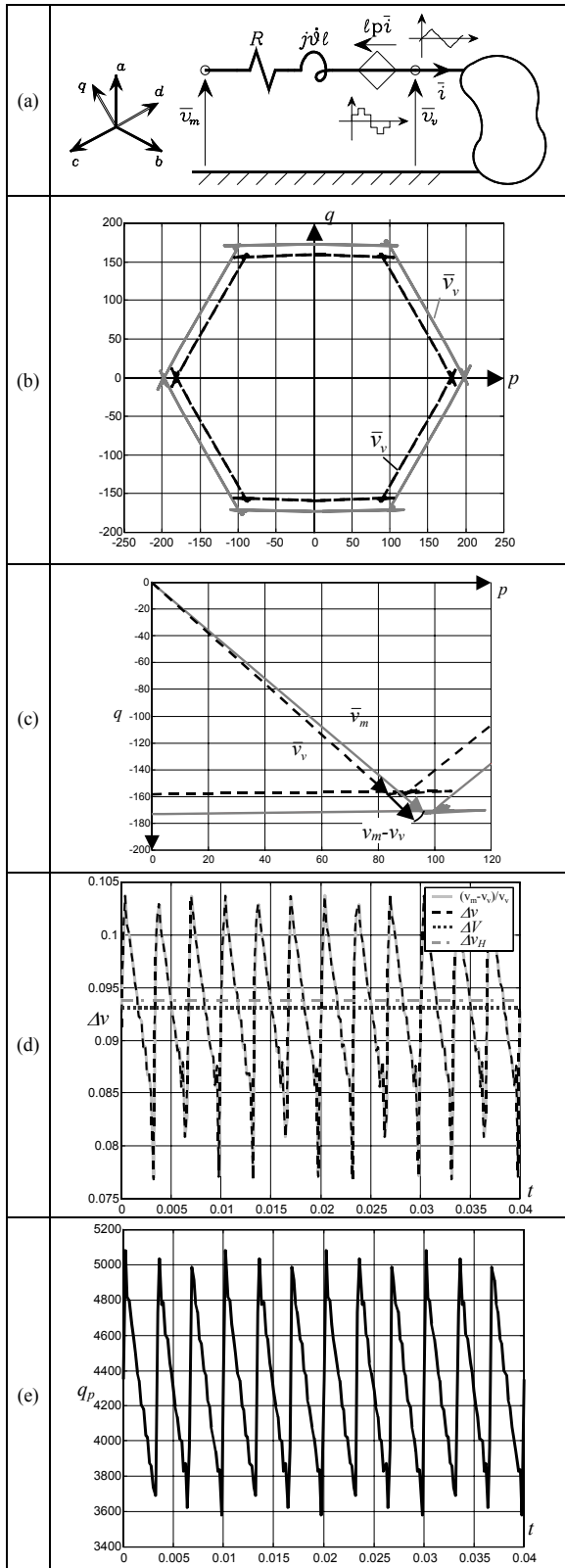


Fig.7. Numerical example where the voltages at the line output port are 6-step waveform. (a) Circuit representation. (b) Polar diagram of Park voltages. \bar{v}_v : Dashed line; \bar{v}_m : solid line. (c) Enlargement of a significant portion of (b) diagram. (d) Voltage drop waveform given by (8), (9), (18) and by a commercial software. (e) Park imaginary power waveform.

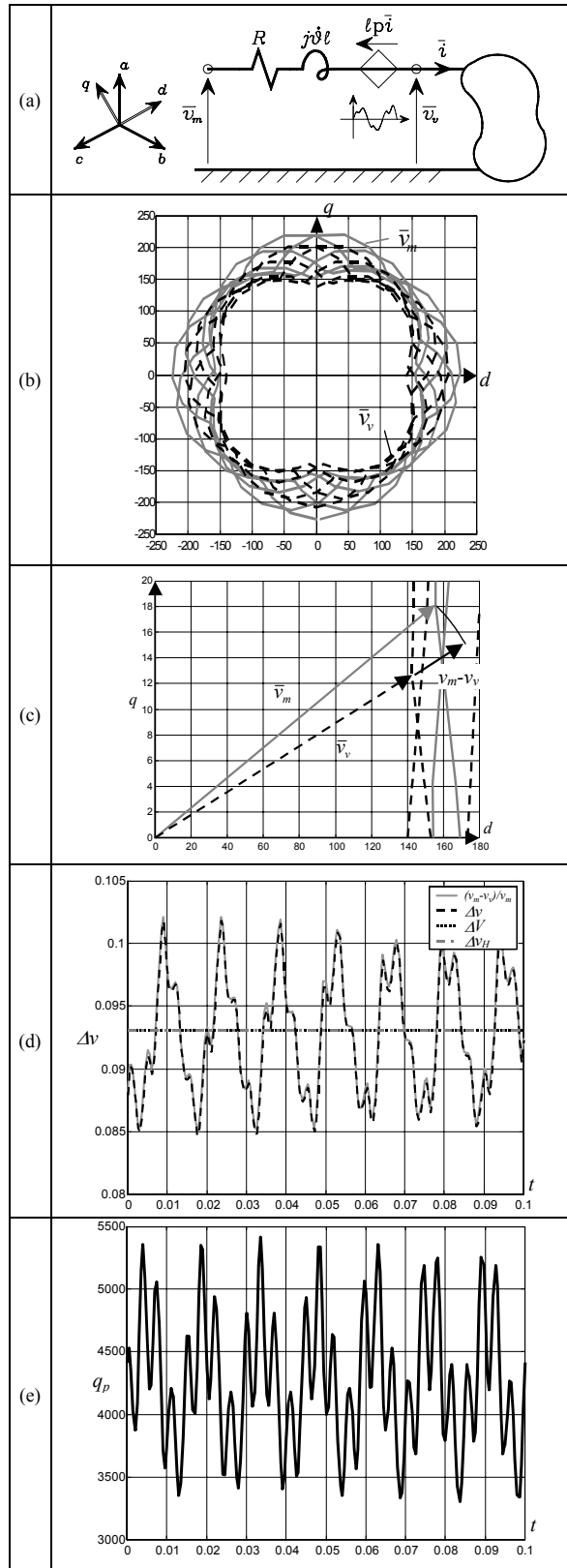


Fig.8. Numerical example where the voltages at the line output port are periodical with subharmonic and interharmonic components. (a) Circuit representation. (b) Polar diagram of Park voltages. \bar{v}_v : Dashed line; \bar{v}_m : solid line. (c) Enlargement of a significant portion of (b) diagram. (d) Voltage drop waveform given by (8), (9), (18) and by a commercial software. (e) Park imaginary power waveform.

This discloses new opportunities to the study of active compensators that can be usefully employed also to control the voltage drop. At last, it is important to underline the role played by the terms $pp_p(t)$, $p\bar{v}_v(t)$: they not only emphasize how synthetic and powerful the Park formalism is, but also confirm the advantage, for energy transmission, to employ a three-phase sinusoidal, symmetric and balanced system.

The obtained results suggest in addition the following comments. Concerning the size of the system components, the use of the classical expression (18) is confirmed. As concern the compensation and stability problems the use of the (9) derived from Park approach is more appropriated giving results on time domain. In this case the imaginary power $q_p(t)$ takes the role of the reactive power Q .

Moreover, since active compensators have been widely studied and are presently available to compensate the imaginary Park power, the proposed analysis also shows a method for practical control of the voltage drop.

APPENDIX A.

The error introduced by using the graphic formulation (5) instead of (2) for evaluating the voltage drop, depends on the ratio between the line and load sequence impedance value as documented in [9].

This error can be evaluated in terms of relative deviation by using the following relationship:

$$\varepsilon\% = (\Delta\bar{v} - \Delta v) / \Delta\bar{v} \cdot 100 \tag{A1}$$

Fig.9 shows the relative deviation $\varepsilon\%$ as a function of the power factor $\cos\varphi$ and of the ratio between the line sequence impedance Z and load sequence impedance Z_L .

Taking into account that the usual value of Z/Z_L in practical cases is less then 0.05 [14], the relative deviation $\varepsilon\%$ is less than 0.5%, the angle δ is less than 2 degrees and the voltage drop is less than 5%.

A relative deviation $\varepsilon\%$ of 2% implies an inductance ratio of 0.25, then a voltage drop (3) close to 27%, a not realistic value for a correct transmission or distribution line design.

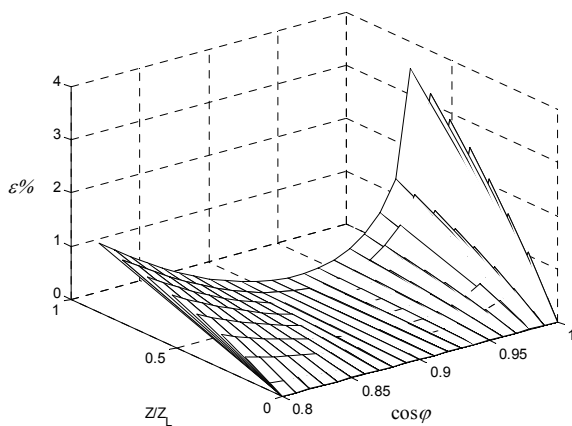


Fig.9. Relative deviation as a function of the ratio Z/Z_L and of the power factor $\cos\varphi$.

APPENDIX B. PARK TRANSFORMATION APPROACH
If the following Park transformation T [2,3] is employed:

$$\begin{cases} [T] = \sqrt{\frac{2}{3}} \cdot \begin{bmatrix} \cos\vartheta_1 & \cos\vartheta_3 & \cos\vartheta_2 \\ -\sin\vartheta_1 & -\sin\vartheta_3 & -\sin\vartheta_2 \\ 1/\sqrt{2} & 1/\sqrt{2} & 1/\sqrt{2} \end{bmatrix} \\ \vartheta_k = \vartheta + (k-1)\frac{2\pi}{3} \quad k=1,2,3 \end{cases} \tag{B1}$$

(B1) can be expressed by means of the $\{d,q,o\}$ variables. Then the Park vectors are defined as (Fig.10):

$$\begin{aligned} \bar{w}(t) &= w_d(t) + jw_q(t) = \\ &= \sqrt{\frac{2}{3}} (w_a(t) + \bar{\alpha}w_b(t) + \bar{\alpha}^2w_c(t)) e^{-j\vartheta(t)} = \bar{w}_{\alpha\beta} e^{-j\vartheta(t)} \end{aligned} \tag{B2}$$

where $\bar{\alpha} = e^{j2\pi/3}$.

The square of the instantaneous rms value of the Park vector can be written in the following form:

$$\begin{aligned} \bar{w}(t)\bar{w}^*(t) &= w_d^2(t) + w_q^2(t) = \bar{w}_{\alpha\beta}(t)\bar{w}_{\alpha\beta}^*(t) = \\ &= \frac{2}{3} [w_a^2(t) + w_b^2(t) + w_c^2(t)] \end{aligned} \tag{B3}$$

that is invariant with the axis choice. The axis can be fixed, $\{\alpha,\beta\}$, or rotating at speed $\dot{\vartheta}$, $\{d,q\}$ (Fig.10). Equation (B3) is a formal time-domain generalization of the rms three-phase value under sinusoidal condition.

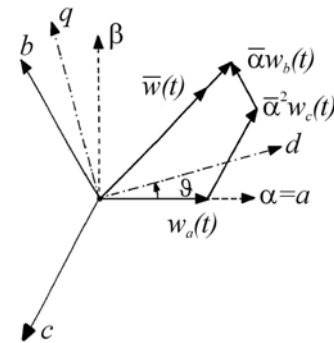


Fig.10. Geometric interpretation of Park transformation.

VIII. REFERENCES

- [1] B. Weedy, Electric Power Systems, London: John Wiley and Sons, third edition 1990
- [2] L. G. Stokvis, Diagramme de la chute de tension dans un conducteur de ligne triphasée de tension moyenne. Cas général d'un système déséquilibré géométriquement et électriquement, Revue Générale de l'Electricité, 1923, pp.3-5
- [3] J. Arrilaga, D.A. Bradley, P.S. Bodger, Power System Harmonics, John Wiley & Sons, 1985. p.116
- [4] A.P. Morando and G. Superti Furga, "Park Power in non sinusoidal three-phase system", l'Energia Elettrica, LXVII, no.2, 1990, pp.65-70, In italian
- [5] A. Ferrero, A.P. Morando, R. Ottoboni and G. Superti Furga, "On the meaning of the Park power components in three-phase system under non

- sinusoidal conditions”, ETEP Eur. Trans. on Electr. Power, vol.3, no. 1, January/February 1993, pp.33-43
- [6] H. Akagi and A. Nabae, “The p-q theory in Three-Phase Systems under non-sinusoidal Conditions”, ETEP Eur. Trans. on Electr. Power 3, no. 1, 1993, pp.27-31
- [7] K. Kupfmüller, Einführung in die theoretische Elektrotechnik, Heidelberg: Springer Verlag, 1968, p.623
- [8] K. Simonyi, Foundations of Electrical Engineering, Oxford: Pergamon Press, 1963, p.385
- [9] A. Ferrero, S. Leva, A.P. Morando, “About the role of the Park Imaginary Power on the Three-Phase Line Voltage Drop”, ETEP Eur. Trans. on Electr. Power 10, no. 5, 2000, pp.287-296
- [10] J. L. Willems, “Mathematical foundations of the instantaneous Power Concepts: a geometrical Approach”, ETEP Eur. Trans. on Electr. Power, Vol.6, no. 5, 1996, pp.299-304
- [11] S. Leva, A.P. Morando, D. Zaninelli, “A New Formulation of Line Voltage Drop in Unbalanced and Distorted Systems”, Proc. of IEEE ICHQP2000, October 1-4, 2000, Orlando (Florida) USA
- [12] S. Leva, A.P. Morando, D. Zaninelli, “Influence of PQ Disturbances on Dynamic Stability of Isolated System”, Proc. of IEEE Power Engineering Society Summer Meeting, 15-19 July, 2002, Vancouver (British Columbia) Canada
- [13] Harmflow+, Harmonic Simulation and Analysis Tools, EPRI/Electrotek, version 2.0, Knoxville (TN), USA, February 1995
- [14] B. Weedy, Electric power systems, London: J. Wiley, 1967

IX. BIOGRAPHIES

Sonia Leva, received the M.S. degree in Electrical Engineering from the “Politecnico di Milano”, Milano, Italy, in 1997. She is now working towards her PhD in Electrical Engineering at the Electrical Engineering Department of the “Politecnico di Milano”. Since 1999 she is Assistant Professor in Elettrotecnica at the same department. Her current research interests are concerned with the electromagnetic compatibility, the power quality and the foundation of electromagnetic theory of electric network.

Adriano Paolo Morando, received the M.S. degree in Electrical Engineering from the “Politecnico di Milano”, Milano, Italy. From 1984 to 1989 he was with ASEA Brown Boveri, where he was concerned with AC drives for electrical traction. Since 1989 he is with the Electrical Engineering Department of the “Politecnico di Milano”. He is now Associated Professor at the same Department. His current research interests are concerned with the electromagnetic compatibility, the power quality and the foundation of electromagnetic theory of electric network.

Dario Zaninelli, received the Ph.D degree in Electrical Engineering from the Politecnico di Milano, in 1989, and he is now Full Professor in the Electrical Engineering Department of the Politecnico di Milano. His areas of research include power system harmonics and power system analysis. Dr. Zaninelli is a senior member of IEEE, a member of AEI and a member of the Italian National Research Council (C.N.R.) group of Electrical Power Systems.

Statistical Evaluation of Voltage Variations via Physically Based Modeling and Simulation

A. P. Sakis Meliopoulos, Fellow and George J. Cokkinides
School of Electrical and Computer Engineering
Georgia Institute of Technology
Atlanta, Georgia 30332-0250
Sakis.meliopoulos@ece.gatech.edu

Andras M. Dan
Department of Electric Power Engineering
Electrical Engineering and Informatics
Budapest University of Technology and Economics
Budapest, Hungary

Abstract:

The majority of power quality problems are associated with voltage variations at the customer site. The voltage variations may be (a) temporary disturbances that may originate anywhere in the system and (b) waveform distortion from nonlinear loads. The sources of disturbances are multiple and with varying parameters. For example in many places of the world, the most frequent disturbances originate from lightning activity near electric installations. Lightning may result in flashover causing voltage sags to some portion of the distribution system, voltage swell to other areas, as well as interruption of power. The number of customers affected depends on the design of the system and placement of interruption devices, while the level of voltage sags or swells may depend on the grounding system, size of neutral, etc. Three-phase distribution systems circuits may consist of 3-wires, 4-wires or 5-wires. Each of these topologies results in different behavior in the presence of disturbances. Furthermore, the advent of distributed generation exacerbates these differences. To properly capture these effects, new system modeling tools are needed that explicitly represent these design details of the system. This paper discusses various modeling methodologies suitable for voltage variation assessment. Since many of the parameters affecting voltage variations are random, emphasis is placed on statistical methods. The modeling approaches discussed include steady state analysis, transient analysis and statistical techniques (Monte Carlo simulation). The methods are demonstrated on a number of example systems.

Introduction

Disturbances that affect power quality are multiple: (a) lightning, (b) switching, (c) power faults, (d) feeder energization inrush currents, (e) motor start, (f) load imbalance, (g) harmonics and resonance, (h) EMI, etc. The effects on the end user could be voltage distortion, voltage sags, voltage swells, outages, voltage imbalance, etc. These effects may have different levels of impact depending on the susceptibility of the end-user equipment. For a specific susceptibility of end-user equipment, the impact of disturbances can be mitigated by design modifications of circuit layout, grounding system design, overvoltage protection, filters, use of steel conduit, use of additional transformers, etc. Traditional power system analysis methods

are based on models that do not capture these phenomena, for example, the most usual models of sequence components do

not predict the voltages in neutrals or grounds and therefore are not appropriate for accurate prediction of voltage variations. This paper proposes a new modeling approach and analysis method for better voltage disturbance evaluation. We address the steady state case as well as transient case.

The proposed method is based on modeling electric power system in their physical configuration, i.e. 3-wire, 4-wire or 5-wire system without the use of any transformations such as the symmetrical component transformation. We also propose a new analysis method for the overall electric power system modeled with physical models. The proposed methodology is capable of modeling systems with three phase wires, four wires (three phase and a neutral/or ground wire), five wires (three phase wires, neutral and a ground wire), single and double phase circuits, grounding and bonding points, grounding systems, etc. Here we discuss analysis methods with these capabilities. The proposed methodology has additional desirable features. For example a physically based model can explicitly represent grounding systems, the size of the neutral wire, the ground wires, etc. These practices have been known to have great effects on power quality. Another important property is that a physically based model and analysis procedure provides the means to expose the interrelationship between the physical parameters and power quality. This property naturally leads to comprehensive cost-benefit analysis.

The paper presents the proposed methodology and provides two practical examples.

Models for Power Quality Assessment

Power quality is affected by design issues such as 3-wire system (three-phase wires), 4-wire system (three-phase wires plus a neutral or ground wire) and 5-wire system (three-phase wires, a neutral and a ground wire), relative size of neutral and ground wires, bonding arrangements, etc. Models for power quality assessment should be able to capture the phenomena occurring in various possible arrangements. It is quite often that the same system may transit from 3-wires into 4-wires, 5-wires and back to 3-wires, etc. In addition, many voltage transformations can occur. Consider for example a typical distribution system consisting a typical overhead distribution

system, underground feeders, electric loads motors, etc. The medium voltage distribution system may be a 4-wire system, some of the secondary voltage circuits may be 5-wire systems, some 3-wire systems, etc. The loading of the system may consist of three phase loads as well as single phase loads. This system may be subjected to a number of disturbances, exogenous such as lightning as well as system internal disturbances such as motor start-up and shutdown, distorting loads, switchings, etc. Typical phenomena to be studied may be transient (lightning, motor start-up, etc.) and/or phenomena that can be described as quasi-steady state, for example, conditions during faults, imbalances, etc. In this section, we present modeling and analysis methodologies that are applicable to these systems and capable of capturing the phenomena that affect power quality. We present time domain analysis methods as well as steady state analysis methods. The common part of the proposed methodologies is the general model of the system that accommodates 3-wire, 4-wire and 5-wire subsystems interconnected in any arbitrary fashion. Specifically, a unified time and frequency domain modeling approach is proposed, using a specific modeling principle. The modeling principle results in physically based quadratized component models and the use of Newton's method to obtain the network solution. A brief description of the method (both frequency domain and time domain) is presented next.

Time Domain Analysis: Any power system device is described with a set of algebraic-differential-integral equations. These equations are obtained directly from the physical construction of the device. It is always possible to cast these equations in the following general form:

$$\begin{bmatrix} \dot{i} \\ 0 \end{bmatrix} = \begin{bmatrix} f_1(\dot{v}, \dot{y}, v, y, u) \\ f_2(\dot{v}, \dot{y}, v, y, u) \end{bmatrix} \quad (1)$$

where i : vector of terminal currents,
 v : vector of terminal voltages,
 y : vector of device internal state variables
 u : vector of independent controls.

Note that this form includes two sets of equations, which are named *external equations* and *internal equations* respectively. The terminal currents appear only in the external equations. Similarly, the device states consist of two sets: *external states* (i.e. terminal voltages, $v(t)$) and *internal states* (i.e. $y(t)$). The set of equations (1) is consistent in the sense that the number of external states and the number of internal equations equals the number of external and internal equations respectively.

Note that equation (1) may contain linear and nonlinear terms. Equation (1) is quadratized, i.e. it is converted into a set of quadratic equations by introducing a series of intermediate variables and expressing the nonlinear components in terms of a series of quadratic terms. The resulting equations are integrated using a suitable numerical integration method. Assuming an integration time step h , the

result of the integration is given with a second order equation of the form:

$$\begin{bmatrix} i(t) \\ 0 \end{bmatrix} = \begin{bmatrix} a_{11} & a_{12} \\ a_{21} & a_{22} \end{bmatrix} \begin{bmatrix} v(t) \\ y(t) \end{bmatrix} + \begin{bmatrix} (v^T(t), y^T(t))F_1 \\ (v^T(t), y^T(t))F_2 \\ \vdots \end{bmatrix} \begin{bmatrix} v(t) \\ y(t) \end{bmatrix} + \begin{bmatrix} b_1(t-h) \\ b_2(t-h) \end{bmatrix} \quad (2)$$

where $b_1(t-h)$, $b_2(t-h)$ are past history functions.

The network solution is obtained by application of Kirchoff's current law at each node of the system (connectivity constraints). This procedure results in the set of equations (3). To these equations, the internal equations are appended resulting to the following set of equations:

$$\sum_k A^k i^k(t) = I_{inj} \quad (3)$$

$$\text{internal equations of all devices} \quad (4)$$

where I_{inj} is a vector of nodal current injections (external injections), A^k is a component incidence matrix with:

$$\{A_{ij}^k\} = \begin{cases} 1, & \text{if node } j \text{ of component } k \text{ is connected to node } i \\ 0, & \text{otherwise} \end{cases}$$

$i^k(t)$ is the vector of terminal currents of component k .

Note that Equations (3) correspond one-to-one with the external system states while Equations (4) correspond one-to-one with the internal system states. The vector $v^k(t)$ of component k terminal voltages is related to the nodal voltage vector $v(t)$ by:

$$v^k(t) = (A^k)^T v(t) \quad (5)$$

Upon substitution of device equations (2), the set of equations (3) and (4) become a set of quadratic equations:

$$Ax(t) + \begin{bmatrix} x^T(t)B_1(t)x(t) \\ x^T(t)B_2(t)x(t) \\ \vdots \end{bmatrix} + b(t-h) = 0 \quad (6)$$

where $x(t)$ is the vector of all external and internal system states.

These equations are solved using Newton's method. Specifically, the solution is given by the following expression.

$$x^{v+1}(t) = x^v(t) - J^{-1}(Ax^v(t) + \begin{bmatrix} x^{vT}(t)B_1(t)x^v(t) \\ x^{vT}(t)B_2(t)x^v(t) \\ \vdots \end{bmatrix} + b(t-h)) \quad (7)$$

where: J is the jacobian matrix of equations (6) and $x^v(t)$ are the values of the state variables at the previous iteration.

Frequency Domain Analysis: Starting from the quadratized equations (1) and assuming that the device operates under steady state (single frequency) conditions, equations (1) are transformed into the following set of complex equations:

$$\begin{bmatrix} \tilde{I}^k \\ 0 \end{bmatrix} = y_{eq_cmpx}^k \begin{bmatrix} \tilde{V}^k \\ \tilde{Y}^k \end{bmatrix} + F \left\{ \begin{bmatrix} x^{kT} f_{eq_real1} x^k \\ x^{kT} f_{eq_real2} x^k \\ \vdots \end{bmatrix} \right\} - b_{eq_cmpx}^k \quad (8)$$

Where \tilde{I}^k : vector of terminal currents,

\tilde{V}^k : vector of terminal voltages,

\tilde{Y}^k : vector of device internal state variables,

$$\tilde{X}^k = \begin{bmatrix} \tilde{V}^k & \tilde{Y}^k \end{bmatrix}^T,$$

x^k = vector \tilde{X}^k in cartesian Coordinates

and $y_{eq_cmpx}^k$, $b_{eq_cmpx}^k$, and $f_{eq_real}^k$ are matrices with

appropriate dimensions. $F(\bullet)$ denotes a function mapping from a real vector to a complex vector. Note that this form includes two sets of equations, which are named *external equations* and *internal equations* respectively. The terminal currents appear only in the external equations. Similarly, the device states consist of two sets: *external states* (i.e. terminal voltages, \tilde{V}^k) and *internal states* \tilde{Y}^k . The set of equations (8) is consistent in the sense that the number of external states and the number of internal states equals the number of external and internal equations respectively. The form of equations (8) resembles the Norton form for electrical components. For this reason we have named the model (8) the Generalized Norton Form (GNF).

The network equations are obtained by application of the connectivity constraints among components. For electrical circuits, the connectivity constraints are simply Kirchoff's current law at each node of the system. This procedure results in the set of equations (9). To these equations, the internal equations are appended resulting in the set of equations (9) and (10):

$$\sum_k A^k \tilde{I}^k = 0 \quad (9)$$

$$\text{internal equations of all devices} \quad (10)$$

where \tilde{I}^k is component k terminal currents composed of the currents at the composite nodes $k1, k2$, etc. A^k is a component incidence matrix. This matrix has been defined earlier.

Let \tilde{V} be the vector of voltages at all the nodes of the system grouped by composite nodes. Then, the following relationship holds:

$$\tilde{V}^k = (A^k)^T \tilde{V} \quad (11)$$

where \tilde{V}^k is component k terminal voltages. Upon substitution of device equations (1) and incidence equations (11), the set of equations (9) and (10) become a set of quadratic equations:

$$\tilde{Y} \tilde{X} + F \begin{bmatrix} x^T f_1 x \\ x^T f_2 x \\ \vdots \end{bmatrix} - \tilde{B} = 0 \quad (12)$$

where \tilde{X} is the vector of states composed of all the components' state \tilde{X}^k ; x is the vector of network states composed of all the components' state x^k ; \tilde{Y} , f , B , etc., are matrices with appropriate dimensions. These equations are the network equations. The simultaneous solution of these equations is obtained via Newton's method described next.

The numerical algorithm for solving the network equations (12) consists of two steps. First, we convert the network equations (12) into cartesian coordinates by simply replacing each complex variable with its cartesian form and separating the real and imaginary parts of the complex equations. The procedure is equivalent with replacing each element in \tilde{Y} with its corresponding 2×2 Hermetian matrix. In particular, \tilde{Y}_{ij} is replaced by:

$$\begin{bmatrix} \tilde{Y}_{ij}^r & -\tilde{Y}_{ij}^i \\ \tilde{Y}_{ij}^i & \tilde{Y}_{ij}^r \end{bmatrix}$$

where superscript r denotes real part and superscript i denotes imaginary part. Then, equation (12) is transformed into Equation (13) below:

$$Y_{real} x + \begin{bmatrix} x^T f_1 x \\ x^T f_2 x \\ \vdots \end{bmatrix} - B_{real} = 0 \quad (13)$$

Equation (13) is solved using Newton's method. Specifically, the solution is given by the following algorithm:

$$x^{v+1} = x^v - J^{-1} \left\{ Y_{real} x^v + \begin{bmatrix} x^{vT} f_1 x^v \\ x^{vT} f_2 x^v \\ \vdots \end{bmatrix} - B_{real} \right\} \quad (14)$$

where v is the iteration step number; J is the Jacobian matrix of equations (13). In particular, the Jacobian matrix takes the following form:

$$J = Y_{real} + \begin{bmatrix} x^{vT} (f_1 + f_1^T) \\ x^{vT} (f_2 + f_2^T) \\ \vdots \end{bmatrix}$$

Algorithm (14) guarantees quadratic convergence since it is Newton’s method applied to a set of quadratic equations. In fact, algorithm (14) converges in two or three iterations.

Applications

The proposed methodologies have been implemented and their application for power quality analysis is described next. We focus on voltage variations and specifically the distribution of voltage disturbances and how they are related to design parameters.

Example Test System: Figure 1 illustrates the example system. Note that it is a small section of a typical distribution circuit with voltage correction capacitors placed at specific points of the system. Note also that the grounding of the system is modeled.

Voltage Sags and Swells: Sequences of fault initiation, fault clearing and reclosing result in voltage sags for certain customers and voltage swells for others. The level of the voltage swells and sags depends on grounding system design. This fact had been recognized long time ago. For example, an IEEE committee has published expected values of overvoltages on unfaulted phases during a ground fault. Similarly, international standards have published similar results. These calculations have been based on power system models that assumed symmetry (symmetrical components). Because the power system components are not symmetric, the voltage swells that will appear in unfaulted phases are different from what the symmetric models predict. The method presented in this paper provides the exact voltage swells and voltage sags for any fault at any location and for any design system in terms of neutral size, grounding design, etc. As an example, Figure 4 illustrates the voltage swells and sags along a circuit during a single line to ground fault. Note that the two unfaulted phases experience a different level of voltage swells due to the asymmetry of the system.

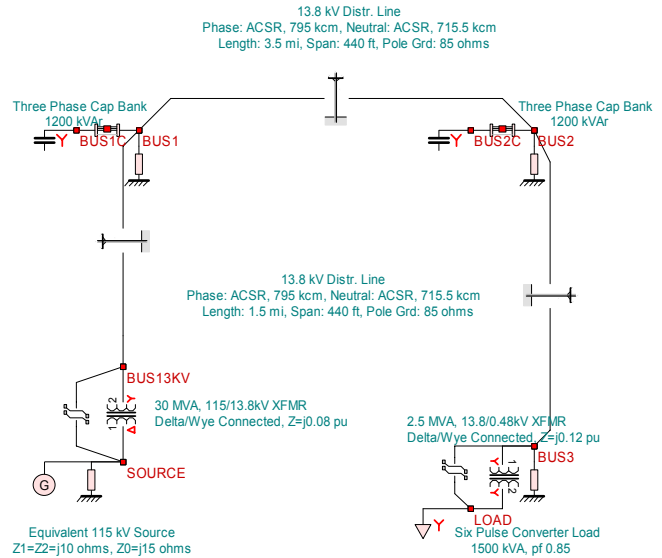


Figure 1. Example Test System for Harmonic Resonance
 The faulted phase experiences voltages sags that vary along the length of the circuit. Figure 4 illustrates the voltages with respect to the neutral. Figure 5 illustrates the absolute voltages of the same phases and same fault condition as well as the voltage of the neutral. Note that the neutral voltage varies along the length of the circuit. It is also important to note here that the absolute voltage swells of the unfaulted phases are lower than the voltage swells relative to the neutral. The difference is due to the voltage elevation of the neutral due to the ground fault. The level of the neutral voltage elevation is dependent upon the design of the grounding system. What is more important is the statistical distribution of the voltage swells or voltage sags for various types of faults that may occur in the system. This topic is discussed next.

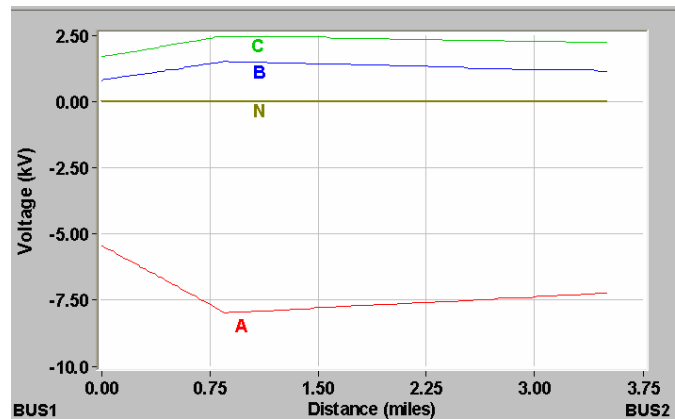


Figure 4. Distribution of Voltage Swells and Sags for a Specific Fault Condition and Circuit Design – Deviation from Nominal, Voltages to Neutral

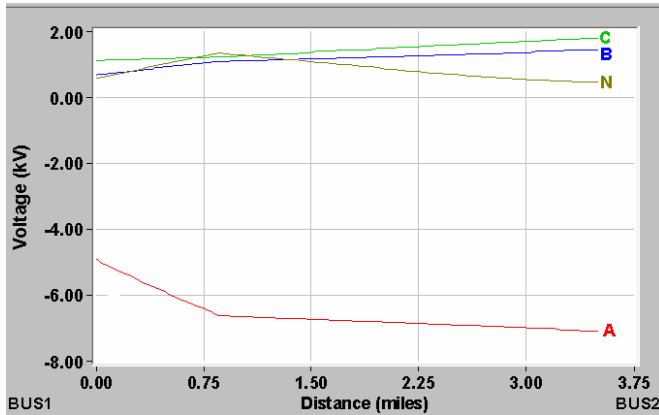


Figure 5. Distribution of Voltage Swells and Sags for a Specific Fault Condition and Circuit Design – Deviation from Nominal, Absolute Voltages

A powerful method to statistically assess the performance of the system relative to power quality is the Monte Carlo simulation. For this purpose, probability distribution functions of random events must be modeled. Then the method consists of the following procedure: first an event is selected (randomly from the known distributions). Then, the condition is simulated and the effects of the condition on power quality are quantified. The procedure is repeated many-many times and the results are summarized into statistical distribution of maximum overvoltages or current at any selected point in the circuit or as a maximum violation of a criterion, etc. The method is applied to determine the statistical distribution of voltage swells and sags. Specifically, the test system of Figure 1 has been used to illustrate the computation of voltage sags and swells distribution using a Monte Carlo simulation. For this purpose, an electric fault type is randomly selected (phase A to neutral, Phase A to Phase B, etc), the fault is applied to a randomly selected location of the system (along any circuit) and the condition is simulated to determine the voltage at a specific customer point. The process is repeated many-many times and the results are tabulated into a probability density function, or a cumulative distribution function. Figure 6 illustrates the results of this simulation for a customer location at BUS2. Note there is substantial probability for voltage sags to the range (0 to 2 kV) and another substantial probability for voltage swells in the range (8 kV to 11 kV). Figure 7 illustrates the probability density function of the absolute voltages. Note the difference that is mainly due to the voltage elevation of the neutral during faults. The proposed model provides a quantitative method to assess this effect.

Transient Voltage Disturbances: Switchings and lightning can initiate transients that propagate through the system and reach sensitive customer equipment. The described time domain simulation method computes the transients reaching any point of the system. Thus the transient voltage waveforms at specific devices terminals are computed and can be compared to the withstand capability (susceptibility curve) of the equipment. This procedure is illustrated in Figures 8 and 9. Figure 8 illustrates the system, the disturbance and the calculation of the transient voltage waveforms. Figure 9

illustrates the identification of the frequency and duration content of the waveform and the placement of the disturbance on the susceptibility curve of the equipment. In this way one can determine, by inspection, the effect of the disturbance on the equipment. Note that the computation procedure requires two components: (a) transient voltage computation by means of system-wide disturbance analysis, and (b) characterization of the disturbance at a specific site in terms of frequency content and peak value.

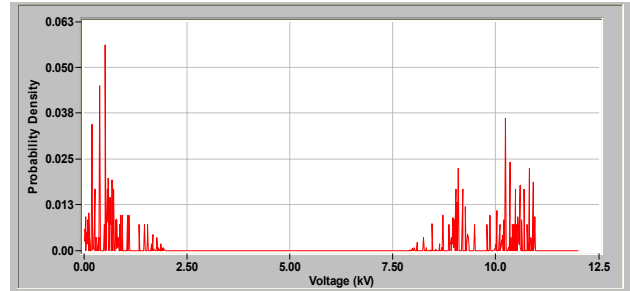


Figure 6. Probability Density Function of Voltages (Phase to Neutral) at BUS2

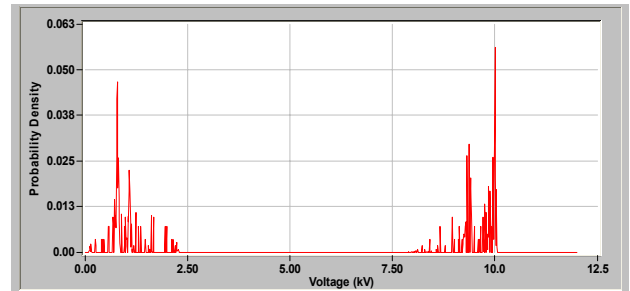


Figure 7. Probability Density Function of Voltages (Absolute Voltages) at BUS2

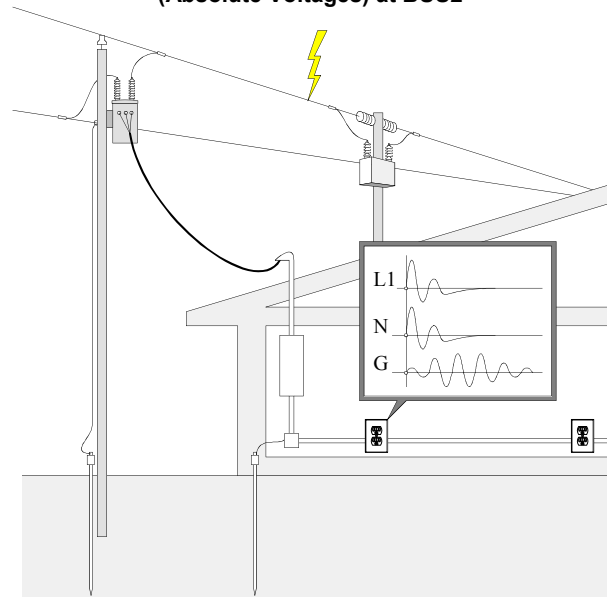


Figure 8. Time Domain Simulation of Transient Voltages

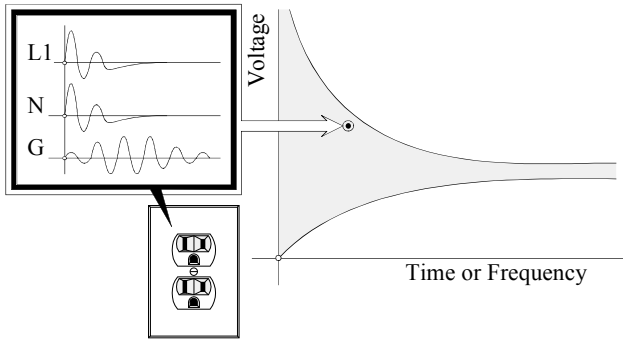


Figure 9. Disturbance Characterization Relative to the Susceptibility Curve

The transient disturbances can occur in many different forms and they are dependent upon parameters that exhibit random variations, such as lightning crest and rise time, switching time relative to the power frequency cycle, etc. For these reasons, it is important to evaluate the transients under all possible variations of the important parameters. A useful method for this purpose is the Monte Carlo simulation described earlier. The Monte Carlo simulation is applied to an example system for the purpose of providing the distribution of transient voltages due to lightning and their relationship to the susceptibility curve of a specific end use equipment.

The example system is illustrated in Figure 10. The system consists of an industrial facility with electronic equipment. It is fed from an overhead 12 kV distribution circuit via a 0.5 mile underground distribution cable. The facility has a ground loop around the building and the transformer neutral is bonded to the ground loop.

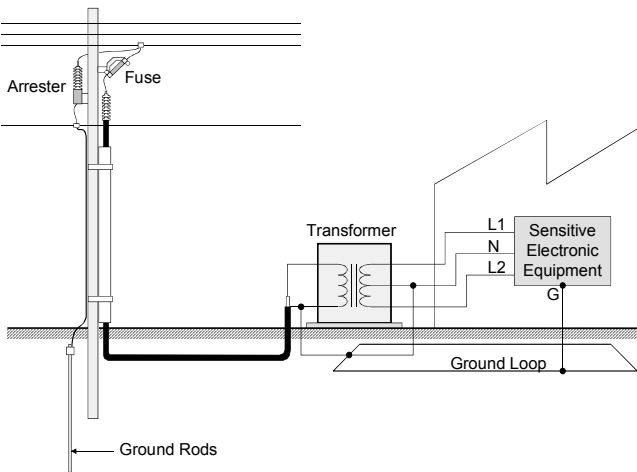


Figure 10. Disturbance Characterization Relative to the Susceptibility Curve

The system of Figure 10 has been evaluated with a Monte Carlo simulation. The point of interest is the sensitive electronic equipment illustrated in Figure 10. A large number of lightning and switching trials have been simulated and the transients at the terminals of the electronic equipment have been recorded, characterized and superimposed on the susceptibility curve. The results are illustrated in Figure 11. The results illustrate that there are two clusters of

overvoltages, one resulting from lightning and another resulting from switching. The results also provide information on the magnitude of these disturbances as related to the susceptibility of the electronic apparatus. One view of the results of Figure 11 is enough to realize that there is a significant number of events that will result in power quality problems for this system. It should be also apparent that the method can be used to assess the effectiveness of specific design modifications on improving the power quality of the system. For example, the grounding of the facility and the 0.5 mile long cable can be modified (improved) by adding another ground conductor. Then the Monte Carlo simulation can be repeated. The performance gains then can be assessed and the cost effectiveness of the design modification can be quantified.

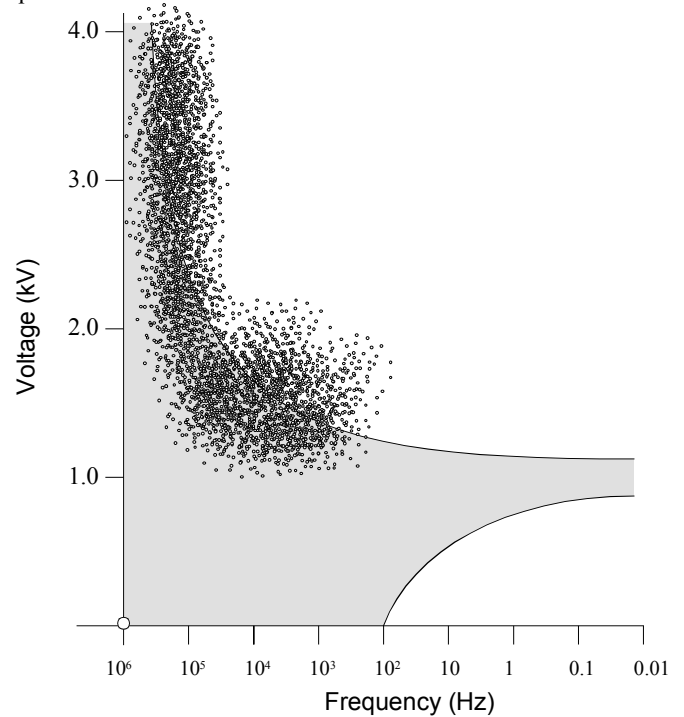


Figure 11. Statistical distribution of Disturbance Voltages Relative to the Susceptibility Curve

Needs and Future Developments

The electric power system is continuously evolving. Recent emphasis is in distributed generation. At the same time, most power quality problems are associated with secondary distribution systems, i.e. systems operating at 480 volts or 2x120 volts. Distributed generation has the potential to contribute a fair amount of power quality problems or to provide nice solutions for premium power quality. For example, most newer distributed generation systems are interfaced to the system via power electronic devices that have the capability to provide additional controls to the system, for example to control the level of imbalance in the system, the neutral voltage under normal operating conditions (stray voltages), etc. It is important to address these issues and the

associated design problems with new methodologies that help to understand the behavior of the system and to provide appropriate solutions. In addition to voltage disturbances, one should be concerned with the stability properties of the system, the capability of distributed generation to maintain synchronism under voltage disturbances and a host of other problems. The proposed methodology is a start towards addressing these issues. We expect that the proposed modeling and analysis methodologies will result in better tools for power quality assessment and improvements in the new complex electric power systems.

Summary and Conclusions

This paper presented a physically based modeling and analysis method of power systems with explicit representation of 3-wire, 4-wire and 5-wire systems. The method provides frequency domain solutions as well as time domain solutions. The model can be used to evaluate typical power quality problems on distribution systems. Because the modeling is physically based, one can directly relate design parameters to power quality performance of the system. Application examples have been presented that clearly correlate power quality performance to the design of the system.

References

1. A. P. Sakis Meliopoulos and G. J. Cokkinides, "A Time Domain Model for Flicker Analysis", *Proceedings of the IPST '97*, pp 365-368, Seattle, WA, June 1997.
2. Eugene V. Solodovnik, George J. Cokkinides and A. P. Sakis Meliopoulos, "Comparison of Implicit and Explicit Integration Techniques on the Non-Ideal Transformer Example", *Proceedings of the Thirtieth Southeastern Symposium on System Theory*, pp. 32-37, West Virginia, March 1998
3. Beides, H., Meliopoulos, A. P. and Zhang, F. "Modeling and Analysis of Power System Under Periodic Steady State Controls", *IEEE 35th Midwest Symposium on Circuit and Systems*
4. IEEE Std 141-1986, IEEE Recommended Practice for Electric Power Distribution for Industrial Plants.
5. IEEE Std 1159-1995, IEEE Recommended Practice for Monitoring Electric Power Quality.
6. IEEE Std 1250-1995, IEEE Guide for Service to Equipment Sensitive to Momentary Voltage Disturbances.
7. ANSI/IEEE Std 519-1981, IEEE Guide for Harmonic Control and Reactive Compensation of Static Power Converters.
8. A. P. Sakis Meliopoulos, "Impact of Grounding System Design on Power Quality", *IEEE Power Engineering Review*, Vol 21, No. 11, pp 3-7, November 2001.
9. Sakis Meliopoulos, "State Estimation for Mega RTOs", *Proceedings of the 2002 IEEE/PES Winter Meeting*, New York, NY, Jan 28-31, 2002.
10. A. P. Sakis Meliopoulos, G. J. Cokkinides and Robert Lasseter, "An Advanced Model for Simulation and Design of Distributed Generation Systems", *Proceedings of MedPower 2002*, Athens, Greece, Nov 3-5, 2002.

Acknowledgments

The work reported in this paper has been partially supported by the ONR Grant No. N00014-96-1-0926 and partially by PSERC/CERTS. This support is gratefully acknowledged.

Biographies

A. P. Sakis Meliopoulos (M '76, SM '83, F '93) was born in Katerini, Greece, in 1949. He received the M.E. and E.E. diploma from the National Technical University of Athens, Greece, in 1972; the M.S.E.E. and Ph.D. degrees from the Georgia Institute of Technology in 1974 and 1976, respectively. In 1971, he worked for Western Electric in Atlanta, Georgia. In 1976, he joined the Faculty of Electrical Engineering, Georgia Institute of Technology, where he is presently a professor. He is active in teaching and research in the general areas of modeling, analysis, and control of power systems. He has made significant contributions to power system grounding, harmonics, and reliability assessment of power systems. He is the author of the books, *Power Systems Grounding and Transients*, Marcel Dekker, June 1988, *Lighning and Overvoltage Protection*, Section 27, *Standard Handbook for Electrical Engineers*, McGraw Hill, 1993, and the monograph, *Numerical Solution Methods of Algebraic Equations*, EPRI monograph series. Dr. Meliopoulos is a member of the Hellenic Society of Professional Engineering and the Sigma Xi.

George J. Cokkinides (M '85) was born in Athens, Greece in 1955. He obtained the B.S., M.S., and Ph.D. degree at the Georgia Institute of Technology in 1978, 1980, and 1985, respectively. From 1983 to 1985, he was a research engineer at the Georgia Tech Research Institute. Since 1985, he has been with the University of South Carolina where he is presently an Associate Professor of Electrical Engineering. His research interests include power system modeling and simulation, power electronics applications, power system harmonics, and measurement instrumentation. Dr. Cokkinides is a member of the IEEE/PES and the Sigma Xi.

András M. Dán (SM'90) received MSc degree from Budapest Technical University in 1966, PhD degree in Electrical Engineering from the Hungarian Academy of Sciences in 1983. He has been at Budapest Technical University since 1970 where he currently holds the rank of professor and acts as a consultant for local industry. His expertise is in power electronics, reactive power compensation especially associated with power system harmonics. Dr Dán is a member of the Hungarian Electrotechnical Association.

Hybrid Fuzzy Logic Control with Global Signals for UPFC to Reduce Control Interactions

L.Y. Dong* and M. L. Crow*

Abstract: In this paper, it is shown that dynamic interactions can occur between multiple UPFCs installed in multimachine power systems. The existence of these dynamic interactions can adversely affect the overall system performance and lead to system instability. To mitigate these adverse interactions, a hybrid fuzzy logic controller for the UPFC is developed. This controller combines the advantages of a fuzzy logic controller and a conventional PI controller. An additional global feedback signal also gives improved performance. The WSCC three-machine system and the IEEE five-machine 14-bus system are used to demonstrate the existence of the control interactions and the efficiency of the proposed approach.

KEYWORDS: Control Interactions, UPFC, Fuzzy Logic

I. INTRODUCTION

The rapid development of the power electronics industry has made FACTS devices attractive for utilities due to their flexibility and capacity of effectively controlling power system dynamics for secure operation. The Unified Power Flow Controller (UPFC) is the most versatile FACTS device, and has the capabilities of controlling power flow in a transmission line, improving transient stability, mitigating system oscillations and providing voltage support [1].

In large interconnected networks, more than one FACTS device in the same region or electrical area will be a natural consequence of the growing use of this technology. However, adverse dynamic interactions can occur not only among the control functions of a single FACTS device but also between different FACTS devices if their controls are not coordinated [2]. The existence of the dynamic interactions among FACTS controls can adversely affect the overall performance and even lead to dynamic instability of the system. Adverse interactions among FACTS controls must be carefully studied and alleviated before multiple FACTS devices can be safely deployed in a system.

Most FACTS device controllers use a conventional proportional-integral (PI) control due to its simplicity. However linear controllers, such as a PI controller, may cause interactions over a wide range of operating conditions or under large disturbances for nonlinear system. To improve the system performance, fuzzy logic theory has been applied to the controller design for FACTS devices. The operation of the fuzzy logic controller does not rely on how accurate the model, parameters, or operating conditions are, but rather, on how effective the linguistic rules of the fuzzy controller are. However, defining membership functions of linguistic variables and formulating fuzzy rules by manual operation are very time consuming. Thus this paper presents a hybrid fuzzy logic controller with global signals for UPFC to minimize the dynamic interactions.

*Electrical and Computer Engineering, University of Missouri-Rolla, Rolla, MO 65409-0040

This controller replaces the proportional term in the conventional PI controller with an incremental fuzzy logic controller while leaving the conventional integral term unchanged. Compared with the existing fuzzy PI controllers, this new hybrid fuzzy proportional plus integral controller keeps the simple structure of the PI controller and can cover a much wider range of operating conditions. To improve the system dynamic stability, additional global control inputs obtained remote from the controller are added into the new hybrid fuzzy controller. Two case studies of the WSCC three-machine system and IEEE five-machine 14-bus system present the efficiency of the proposed hybrid fuzzy logic controller in reducing dynamic control interactions.

II. POWER SYSTEM MODEL

In order to consider the full effects of the generator dynamics including the speed governor and turbine, exciter/AVR and UPFC dynamics, the following dynamic models of the system components were used [3]:

Two-Axis Generator Model:

$$\begin{aligned} \dot{\delta} &= \omega - \omega_s \\ M\dot{\omega} &= T_M + \frac{V}{x'_d} (E'_d \cos(\theta - \delta) + E'_q \sin(\theta - \delta)) \end{aligned}$$

$$T'_{do} \dot{E}_q = -\frac{x_d}{x'_d} E'_q + \frac{x_d - x'_d}{x'_d} V \cos(\theta - \delta) + E_{fd}$$

$$T'_{qo} \dot{E}_d = -\frac{x_q}{x'_q} E'_d + \frac{x_q - x'_q}{x'_q} V \sin(\theta - \delta)$$

(assumption: $x'_d = x'_q$ and $R_s = 0$)

IEEE Type I Exciter/AVR Model:

$$\begin{aligned} T_E \dot{E}_{fd} &= -K_E E_{fd} - S_E (E_{fd}) E_{fd} + V_R \\ T_A \dot{V}_R &= -V_R + K_A \left(R_F - \frac{K_F}{T_F} E_{fd} + V_{ref} - V_T \right) \end{aligned}$$

$$T_F \dot{R}_F = -R_F + \frac{K_F}{T_F} E_{fd}$$

Speed Governor Model

$$T_{SV} \dot{P}_{SV} = -P_{SV} + P_C - \frac{1}{R} \frac{\omega}{\omega_s}$$

Turbine Model

$$T_{RH} \dot{T}_M = -T_M + \left(1 - \frac{K_{HP} T_{RH}}{T_{CH}} \right) P_{CH} + \frac{K_{HP} T_{RH}}{T_{CH}} P_{SV}$$

$$T_{CH} \dot{P}_{CH} = -P_{CH} + P_{SV}$$

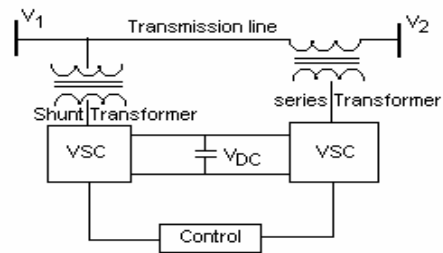


Figure 1: UPFC Schematic diagram

The unified power flow controller, or UPFC, is the most complex voltage-sourced-converter (VSC)-based FACTS device. Figure 1 shows the schematic diagram of a UPFC. It consists of a combination of a shunt and series branches connected through a DC capacitor. The series connected inverter injects a voltage with controllable magnitude and phase angle in series with the transmission line, therefore providing real and reactive power to the transmission line. The shunt-connected inverter provides the real power drawn by the series branch and the losses and can also independently provide reactive compensation to the system by the reactive current [1]. By defining a proper synchronous reference frame, the dynamic model of UPFC can be written as:

$$\begin{aligned} \frac{1}{\omega} \dot{i}_{d1} &= -\frac{R_{s1}}{L_{s1}} i_{d1} + i_{q1} + \frac{k_1}{L_{s1}} \cos(\alpha_1 + \theta_1) V_{dc} - \frac{1}{L_{s1}} V_1 \cos(\theta_1) \\ \frac{1}{\omega} \dot{i}_{q1} &= -\frac{R_{s1}}{L_{s1}} i_{q1} - i_{d1} + \frac{k_1}{L_{s1}} \sin(\alpha_1 + \theta_1) V_{dc} - \frac{1}{L_{s1}} V_1 \sin(\theta_1) \\ \frac{1}{\omega} \dot{i}_{d2} &= -\frac{R_{s2}}{L_{s2}} i_{d2} + i_{q2} + \frac{k_2}{L_{s2}} \cos(\alpha_2 + \theta_1) V_{dc} \\ &\quad - \frac{1}{L_{s2}} (V_2 \cos(\theta_2) - V_1 \cos(\theta_1)) \\ \frac{1}{\omega} \dot{i}_{q2} &= -\frac{R_{s2}}{L_{s2}} i_{q2} - i_{d2} + \frac{k_2}{L_{s2}} \sin(\alpha_2 + \theta_1) V_{dc} \\ &\quad - \frac{1}{L_{s2}} (V_2 \sin(\theta_2) - V_1 \sin(\theta_1)) \\ \frac{C}{\omega} \dot{V}_{dc} &= -k_1 \cos(\alpha_1 + \theta_1) i_{d1} - k_1 \sin(\alpha_1 + \theta_1) i_{q1} \\ &\quad - k_2 \cos(\alpha_2 + \theta_1) i_{d2} - k_2 \sin(\alpha_2 + \theta_1) i_{q2} - \frac{V_{dc}}{R_{dc}} \end{aligned}$$

where i_{di} and i_{qi} are the injected dq converter currents, V_{dc} is the voltage across the DC capacitor, R_{dc} represents the switching losses, $V_1 \angle \theta_1$ and $V_2 \angle \theta_2$ are the terminal voltages of the UPFC.

The power balance equations at bus 1 are given by:

$$\begin{aligned} 0 &= V_1 \left((i_{d1} - i_{d2}) \cos \theta_1 + (i_{q1} - i_{q2}) \sin \theta_1 \right) \\ &\quad - V_1 \sum_{j=1}^n V_j Y_{1j} \cos(\theta_1 - \theta_j - \phi_{1j}) \\ 0 &= V_1 \left((i_{d1} - i_{d2}) \sin \theta_1 - (i_{q1} - i_{q2}) \cos \theta_1 \right) \\ &\quad - V_1 \sum_{j=1}^n V_j Y_{1j} \sin(\theta_1 - \theta_j - \phi_{1j}) \end{aligned}$$

and at bus 2:

$$\begin{aligned} 0 &= V_2 \left((i_{d2}) \cos \theta_2 + (i_{q2}) \sin \theta_2 \right) \\ &\quad - V_2 \sum_{j=1}^n V_j Y_{2j} \cos(\theta_2 - \theta_j - \phi_{2j}) \end{aligned}$$

$$\begin{aligned} 0 &= V_2 \left((i_{d2}) \sin \theta_2 - (i_{q2}) \cos \theta_2 \right) \\ &\quad - V_2 \sum_{j=1}^n V_j Y_{2j} \sin(\theta_2 - \theta_j - \phi_{2j}) \end{aligned}$$

III. CONTROL INTERACTION ANALYSIS

The UPFC has three control parameters: the magnitude and angle of the injected voltage and the shunt reactive current. The series output active and reactive power flow control can be controlled independently by injecting a series voltage with an appropriate magnitude and angle. In the synchronous rotating dq reference frame, the series injected voltage can be split into E_d and E_q . By controlling E_d and E_q properly, different active and reactive power flows can be achieved. Similarly by controlling the shunt injected voltage E_d and E_q , the shunt-connected converter can provide independent reactive power support and maintain constant DC capacitor voltage. The conventional PI technique is typically used in UPFC controller design. One straightforward PI-based control is shown in Figure 2 [4].

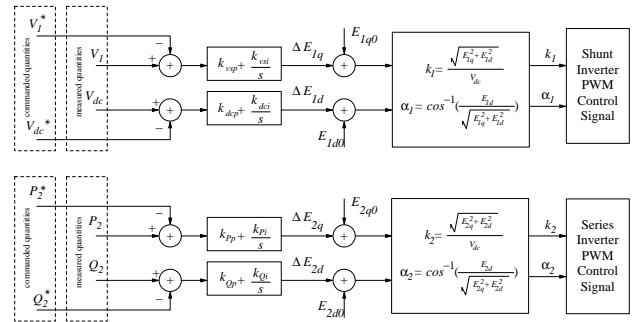


Figure 2: UPFC Control Block Diagram

To investigate the interactions among UPFC controllers, two case studies are presented for the WSCC three-machine nine-bus system and the IEEE five-machine 14-bus system. All the UPFC controllers use the PI-based control approach shown in Figure 2 and each UPFC control is designed and optimized separately without considering the presence of other UPFCs.

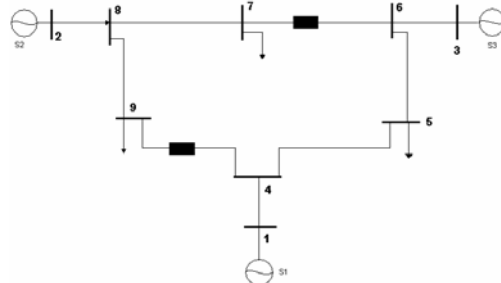


Figure 3: WSCC Three-machine nine-bus System

The WSCC System Example

The WSCC three-machine nine-bus system shown in Figure 3 is adapted to demonstrate the existence of dynamic interactions among UPFC controllers. UPFC₁ and UPFC₂ are installed in transmission lines 6-7 and 4-9 respectively as shown. A three-phase fault is applied at bus 8 to simulate a transient disturbance. The fault is introduced at 0.02s and cleared after 100ms without a system configuration change. The main control tasks of the UPFC are to maintain the steady-state power flow, DC capacitor voltage, and provide voltage support.

Figures 4 through 6 show the dynamic performance of the system with two UPFCs installed. Figure 4 shows the generator frequencies. Figures 5 and 6 show the active and reactive power flows across their respective lines. All of these responses clearly indicate that an instability occurs, although the system is stable when each UPFC controller is independently installed. This is a clear example that shows the existence of the dynamic interactions between the UPFC controllers, which can lead to potential system instability.

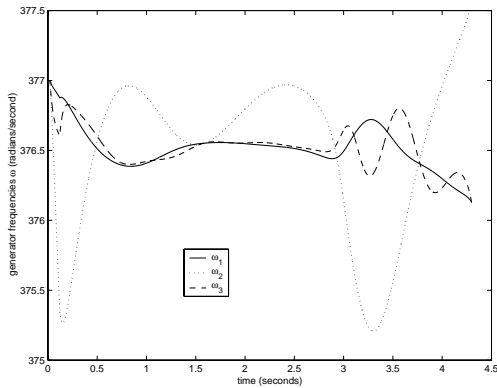


Figure 4: Generator frequencies

To pinpoint which portion of the PI controller is interacting negatively, the simulation of the two UPFC controls with the UPFC₂ series reactive power control **disabled** is shown as the dash-dot lines in Figure 7. The solid lines are the results with the UPFC₂ series reactive power control enabled. Figure 7 clearly indicates that it is the interaction of the reactive power controls that are causing the instability.

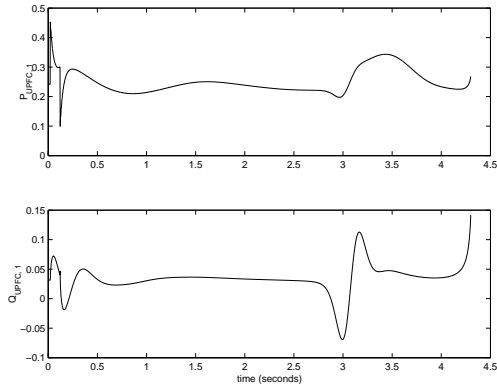


Figure 5: UPFC₁ installed in line 6-7

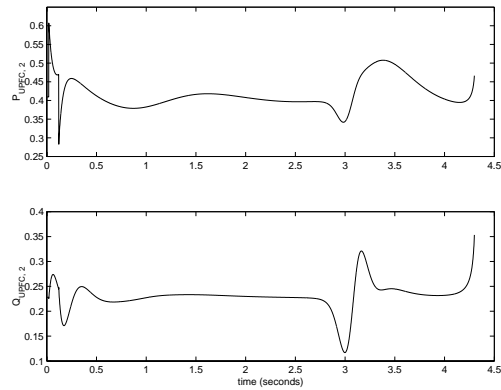


Figure 6: UPFC₂ installed in line 4-9

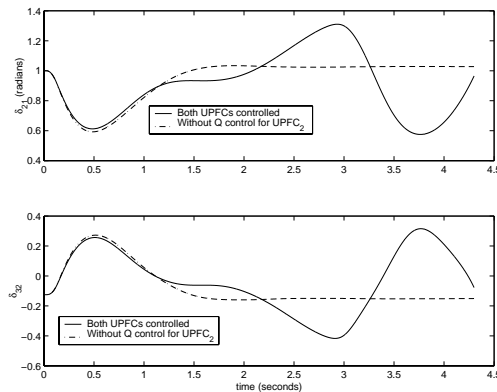


Figure 7: Comparison of the rotor angle differences with and without reactive power controls on UPFC₂

The IEEE 14 Bus System Example

This section presents another case study for control interaction analysis. UPFC₁ and UPFC₂ are installed in transmission line 6-16 and 2-17 respectively of the IEEE 14 bus system as shown in Figure 8. A three-phase fault of 100ms duration is

simulated at bus 8.

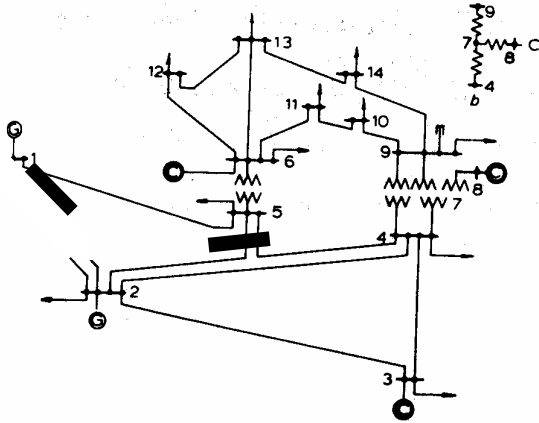


Figure 8: The IEEE five-machine 14-bus System

From Figures 9 and 10, it can be seen that the system exhibits high frequency interactions between these two UPFC controllers. As in the WSCC case, the system is again simulated with the reactive power portion of the UPFC₂ PI controller disabled. As before, when the controller is disabled, the interactions cease to exist.

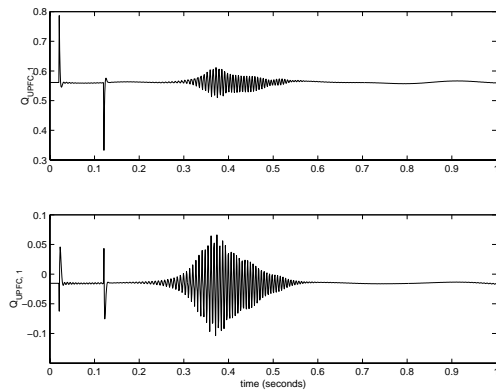


Figure 9: UPFC₁ installed in line 6-16

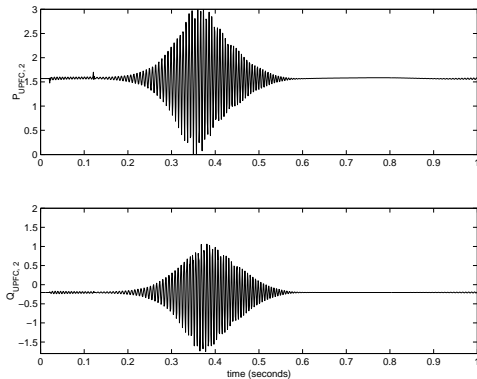


Figure 10: UPFC₂ installed in line 2-17

The case studies presented above demonstrate that there dynamic interactions do exist among UPFC controllers and that a purely linear PI control approach may not properly capture the complex dynamics of the system under large disturbances. To deal with the nonlinearity and uncertainty of the system, a nonlinear hybrid fuzzy logic controller with global signals will be developed in the next session to minimize the dynamic interactions.

IV. HYBRID FUZZY CONTROLLER DESIGN

A conventional PI controller uses an analytical expression of the following form to compute the control action:

$$u(t) = K_p \cdot e(t) + K_I \cdot \int e(t) dt.$$

The discrete-time and incremental form is written as

$$\Delta u(k) = K_p \cdot \Delta e(k) + K_I \cdot T \cdot e(k),$$

where

$\Delta u(k)$ is the change of control output and we have that

$$\Delta u(k) = u(k) - u(k-1),$$

$e(k)$ is the error and $e(k) = y_{sp} - y(k)$, where $y(k)$ is the system output and y_{sp} is the desired system output,

$$\Delta e(k) \text{ is change of error } \Delta e(k) = e(k) - e(k-1),$$

k is the k -th sampling time and T is the sampling time.

The PI controller has a simple control structure and is easy to design by adjusting the two control parameters K_p and K_I to achieve acceptable performance. The main idea of the hybrid fuzzy controller is to use the fuzzy proportional (P) controller to improve the overshoot and rising time response and a conventional integral (I) controller to reduce the steady-state error [5]. Therefore, combining the advantages of a conventional PI controller and a nonlinear fuzzy logic control technique, this controller is constructed by replacing the proportional term in the conventional PI controller with an incremental fuzzy logic controller.

$$\Delta u(k) = u(k) - u(k-1) = K_p \cdot \Delta u_f(k) + K_I \cdot T \cdot e(k)$$

where $\Delta u_f(k)$ is the output of the incremental fuzzy logic controller. This control scheme is shown in Figure 12.

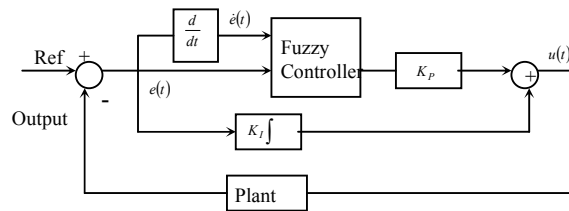


Fig.12 Hybrid Fuzzy control scheme

The main fuzzy logic control procedure is to fuzzify the controller inputs, then infer the proper fuzzy control decision based on defined rules and the fuzzy output is then produced by defuzzifying this inferred control decision.

A. Fuzzification and membership functions

The fuzzification will transfer the crisp control variables to corresponding fuzzy variables. It is common to use the output error and the derivative of the output as controller inputs. Therefore, the incremental fuzzy logic controller selects $e(k)$ and $\dot{e}(k)$ as its inputs in this paper.

Each of the fuzzy logic controller input and output signals is interpreted into a number of linguistic variables and each linguistic variable has its own fuzzy membership function. The membership function maps the crisp values into fuzzy variables. In this hybrid fuzzy controller, membership functions N (negative), Z (zero) and P (positive) assigned with linguistic variables are used to fuzzify the error and its derivative. Inputs $e(k)$ and $\dot{e}(k)$ fuzzify into $(e.n, e.z, e.p)$ and $(\dot{e}.n, \dot{e}.z, \dot{e}.p)$. For the output $\Delta u_f(k)$, $(o.n, o.z, o.p)$ are the fuzzy states. For simplicity, it is assumed that the membership functions are symmetrical and each one overlaps the adjacent functions by 50%. The membership functions for the inputs and the output are shown in Figure 13.

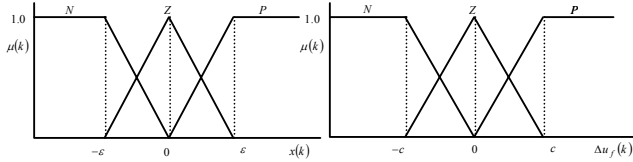


Figure 13: Membership functions for the hybrid fuzzy controller

The membership function of the positive set is

$$\mu_p(x) = \begin{cases} 0 & x < 0 \\ \frac{x}{\varepsilon} & 0 \leq x \leq \varepsilon \\ 1 & x > \varepsilon \end{cases}$$

where $x(k)$ represents the inputs to the fuzzy controller at the k th sampling instant.

The membership function of the negative set is

$$\mu_N(x) = \begin{cases} 1 & x < -\varepsilon \\ -\frac{x}{\varepsilon} & -\varepsilon \leq x \leq 0 \\ \frac{\varepsilon}{\varepsilon - x} & 0 < x \leq \varepsilon \\ 0 & x > \varepsilon \end{cases}$$

And for the zero set the membership function used is

$$\mu_Z(x) = \begin{cases} 0 & x < -\varepsilon \\ \frac{x + \varepsilon}{\varepsilon} & -\varepsilon \leq x \leq 0 \\ \frac{\varepsilon - x}{\varepsilon} & 0 < x \leq \varepsilon \\ 0 & x > \varepsilon \end{cases}$$

B. Rule base and inference

In general, fuzzy systems map input fuzzy sets to output fuzzy sets. Fuzzy rules are used to characterize the relationship between fuzzy inputs and fuzzy outputs. For a system of two control variables with three linguistic variables in each range, this leads to the following 3×3 rules:

- R1: If $e(k)$ is N and $\dot{e}(k)$ is P then $\Delta u_f(k)$ is Z
- R2: If $e(k)$ is Z and $\dot{e}(k)$ is P then $\Delta u_f(k)$ is P
- R3: If $e(k)$ is P and $\dot{e}(k)$ is P then $\Delta u_f(k)$ is P
- R4: If $e(k)$ is N and $\dot{e}(k)$ is Z then $\Delta u_f(k)$ is N
- R5: If $e(k)$ is Z and $\dot{e}(k)$ is Z then $\Delta u_f(k)$ is Z
- R6: If $e(k)$ is P and $\dot{e}(k)$ is Z then $\Delta u_f(k)$ is P
- R7: If $e(k)$ is N and $\dot{e}(k)$ is N then $\Delta u_f(k)$ is N
- R8: If $e(k)$ is Z and $\dot{e}(k)$ is N then $\Delta u_f(k)$ is N
- R9: If $e(k)$ is P and $\dot{e}(k)$ is N then $\Delta u_f(k)$ is Z

Using the inference engine Max-Min and Zadeh's rules for AND, the activation of the i th rule consequence is a scalar value which equals the minimum of the two antecedent conjuncts' values. A defuzzification method is also required to transform fuzzy control activations into a crisp output value. For the incremental fuzzy logic controller, using center of mass defuzzification method the output $\Delta u_f(k)$ is

$$\Delta u_f(k) = \frac{\sum_{j=1}^9 \mu_j \cdot c_j(k)}{\sum_{j=1}^9 \mu_j}$$

where $c_j(k)$ is the value of control output corresponding to the membership value of input equal to unity.

C. A Hybrid Fuzzy Controller for UPFC

The conventional PI control approach for UPFC is divided into both shunt and series portions. The shunt PI controller to provide voltage support and maintain the constant DC capacitor voltage is given by:

$$\Delta E_{1q} = K_{vsP} \Delta V_1 + K_{vsI} \int_0^t \Delta V_1(t) dt$$

$$\Delta E_{1d} = K_{dcP} \Delta V_{dc} + K_{dcI} \int_0^t \Delta V_{dc}(t) dt$$

The series PI controller to regulate the series output active and reactive power is given by:

$$\Delta E_{2q} = K_{pP} \Delta P_2 + K_{pI} \int_0^t \Delta P_2(t) dt$$

$$\Delta E_{2d} = K_{qP} \Delta Q_2 + K_{qI} \int_0^t \Delta Q_2(t) dt$$

To construct the hybrid fuzzy logic controller, the proportional terms in the conventional PI controllers described above are replaced by the output variables of the incremental fuzzy logic controller. Since the series reactive power controller is responsible for the negative interaction in both case studies, the simple conventional PI controller remains for shunt voltage regulation and DC capacitor voltage maintenance. The hybrid fuzzy logic controller is applied for series active and reactive power control only. This reduces the complexity of the control.

D. Additional global signal inputs

The effectiveness in system dynamic stability is limited by using local signals for the controllers. Additional global signal inputs obtained remote from the controller make it possible to get improved performance. From the above case studies, the interactions among UPFC controllers can adversely influence the rotor damping of the generators, thus the difference in speed between two generators are applied as the global signals in this paper. Figure 9 shows the hybrid fuzzy logic control scheme with global signal inputs for the UPFC.

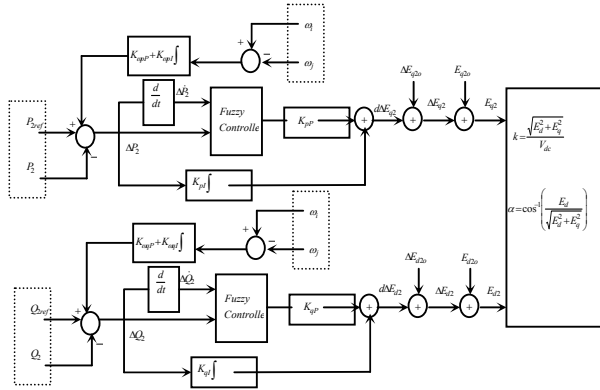


Figure 14: Hybrid Fuzzy Logic Controller with global signal inputs

V. SIMULATION VERIFICATION

The same example systems are used to evaluate the performance of the new hybrid fuzzy logic controller for UPFC in minimizing the dynamic control interactions.

The WSCC Test System

The same three-phase fault with 100ms duration is applied at bus 8 of WSCC three-machine nine-bus system with two UPFCs installed in lines 6-7 and 4-9 respectively.

The speed difference between generators 1 and 2, and generators 2 and 3 are chosen to be the global control signal inputs. With the additional global signal inputs, the series hybrid fuzzy logic controller is rewritten as:

$$\begin{aligned} \Delta E_{2q} &= K_{pP} \left(\Delta P_2 + \sum K_{\omega pPk} (\omega_i - \omega_j) + K_{wplk} \int_0^t (\omega_i - \omega_j) \right) \\ &+ K_{pI} \int_0^t \left(\Delta P_2 + \sum K_{\omega pPk} (\omega_i - \omega_j) + K_{wplk} \int_0^t (\omega_i - \omega_j) \right) dt \\ \Delta E_{2d} &= K_{qP} \left(\Delta Q_2 + \sum K_{\omega qPk} (\omega_i - \omega_j) + K_{wqk} \int_0^t (\omega_i - \omega_j) \right) \\ &+ K_{qI} \int_0^t \left(\Delta Q_2 + \sum K_{\omega qPk} (\omega_i - \omega_j) + K_{wqk} \int_0^t (\omega_i - \omega_j) \right) dt \end{aligned}$$

Figures 15 through 18 show the system dynamic performance comparison by using hybrid fuzzy logic controller with global signals inputs, hybrid fuzzy logic controller only and conventional PI controller respectively. Using a conventional PI controller, the dynamic control interactions occur between the UPFC controllers and lead to the system instability. The adverse interactions cannot be reduced even with the hybrid fuzzy logic controller and the system is still going unstable. By adding the additional global signal inputs, the hybrid fuzzy logic controller minimizes the dynamic interactions and the system returns to a stable state. Therefore, the combination of the hybrid fuzzy logic controller with the additional global signal inputs is the most efficient approach to eliminate the control interactions.

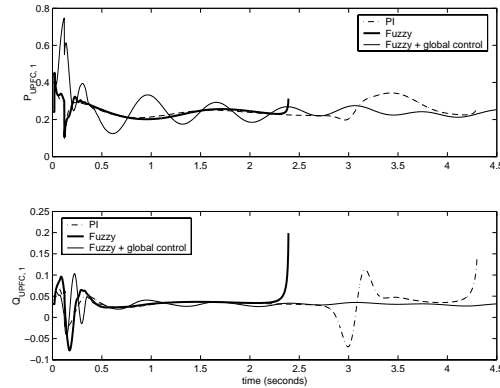


Figure 15: UPFC₁ active and reactive power responses

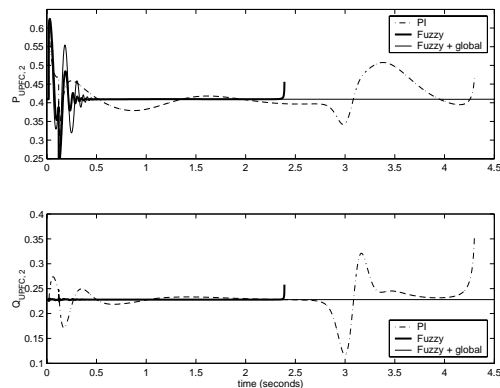


Figure 16: UPFC₂ active and reactive power responses

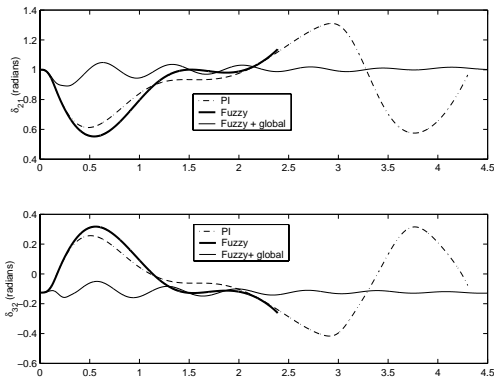


Figure 17: Generator angle differences

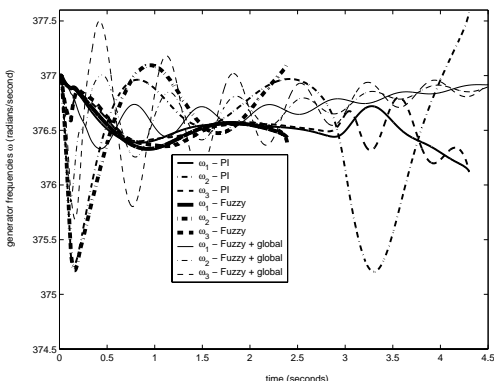


Figure 18: Generator frequencies

The IEEE 14 bus test system

To validate the robustness of the hybrid fuzzy logic controller with global signal inputs, the IEEE five-machine 14-bus system is used with UPFC₁ and UPFC₂ installed in lines 6-16 and 2-17 respectively. The same three-phase fault of 100ms duration is simulated at bus 8. The results of the global hybrid fuzzy control are shown together with the conventional PI control results in Figure 19 and 20. In this case it can also demonstrate that the new global hybrid fuzzy control approach has a satisfactory performance on the elimination of control interactions.

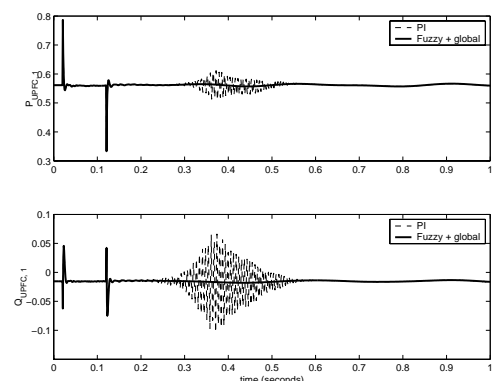


Figure 19: UPFC₁ active and reactive power responses

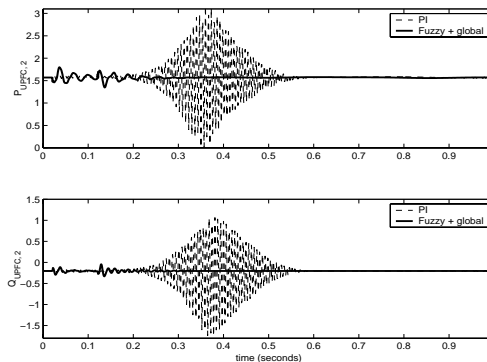


Figure 20: UPFC₂ active and reactive power responses

VI. CONCLUSIONS

This paper investigates the existence of dynamic interactions between multiple UPFC controllers. Due to the interactions, the joint operation of the UPFC controllers can result in poor control performance and even a closed-loop system instability. Therefore, a new hybrid fuzzy logic control is presented for UPFC to reduce the dynamic control interactions. The structure of the fuzzy controller is very simple since it only replaces the proportional term of the conventional PI controller in an incremental fuzzy logic controller and remains the conventional integral term. This paper also shows the improved dynamic system stability performance that is achieved by adding additional global control signals to the hybrid fuzzy controller.

REFERENCES

- [1] L. Gyugi, "Unified Power Flow concept for flexible AC transmission systems," IEE Proc. C, vol. 139, no. 4, 1992.
- [2] Pilotto, L.A.S.; Long, W.F.; Edris, A.A., "Basic mechanisms of control interactions among power electronic-assisted power systems," *Transmission and Distribution Conference and Exposition*, 2001 IEEE/PES.
- [3] P. Sauer and M. A. Pai, *Power System Dynamics and Stability*, McGraw-Hill, 1998.
- [4] L. Dong, M. Crow, Z. Yang, and L. Zhang, "A Reconfigurable FACTS System for University Laboratories," *IEEE Trans for Power Systems*, in review.
- [5] Driankov, Dimitar, "An Introduction to Fuzzy Control," Springer-Verlag Berlin Heidelberg 1993

L. Y. Dong is currently a Ph.D. candidate in the Electrical and Computer Engineering department at the University of Missouri-Rolla. Her research interests include FACTS device control, interaction, placement and power system stability.

M. L. Crow is presently the Associate Dean for Research and Graduate Affairs and a professor of Electrical and Computer Engineering at the University of Missouri-Rolla. Her area of research interests have concentrated on the application of power electronics in bulk power systems. She is the Vice-President for Education/Industry relations of the Power Engineering Society.

Some Comments on Power Acceptability Curves

G. Heydt
 Arizona State University
 Tempe, Arizona USA

R. Thallam
 Salt River Project
 Phoenix, Arizona USA

M. Albu
 Universitatea Politehnica București
 Bucharest, Romania

Abstract

Power acceptability curves, also known as voltage vulnerability or sensitivity curves, have been used for over 30 years to characterize momentary events of low voltage in power distribution systems. In this paper, a summary of how the curves were developed is given, and some thoughts on the applicability of the curves are presented.

Index terms: CBEMA curve, voltage sags, power quality, power acceptability, voltage sensitivity

I. Power acceptability

Many power quality indices relate to steady state phenomena, and relatively few relate to momentary events. However, many power quality engineers feel that bus voltage sags, a natural consequence of a highly interconnected transmission system, may be the most important type of power quality degradation, and therefore a useful measure of the severity of these events is desirable. One such metric is the power acceptability curve (or voltage sensitivity or voltage vulnerability curve) which is a graphic metric of the severity of bus voltage sags plotted versus the duration of these events. Table I shows some of the issues that might be captured by a power acceptability (sensitivity) metric.

The best known of the graphical metrics for bus voltage sensitivity is the Computer Business Equipment Manufacturing Association (CBEMA) curve which is a graphic depicting the severity of a distribution bus voltage sag, ΔV , versus its duration T . The ΔV - T plane is a two dimensional space in which the line $\Delta V = 0$ represents the case that distribution voltage is at rated value, and the $\Delta V < 0$ half-plane is the bus voltage sag region. Overvoltage and undervoltage events of very minimal impact (small $|\Delta V|$) are considered 'acceptable' in the sense that loads are not disrupted; further, very short duration events (small T) are considered acceptable. Thus the ΔV - T plane is divided into *acceptable* and *unacceptable* regions. Fig. (1) shows the CBEMA power acceptability curve. The CBEMA curve depicted in Fig. (1) has ΔV indicated as

a percent of rated voltage, and T shown on a logarithmic scale in seconds.

Table I Some issues in voltage sag and overvoltage events in primary distribution systems

Type of event	Root cause	Main issues to be captured by an event that measures the metric
Overvoltage	High voltage circuit in contact with low voltage circuit	$ \Delta V $
	Inappropriate shunt capacitor application	$ \Delta V $
	Capacitor switching	$ \Delta V $, crest factor, duration of event
Low voltage	Induction motor startup	$ \Delta V $, duration of event, possibly phase shift during event
	Heavy pulsating loads, heavily loaded feeders	$ \Delta V $, duration of event
	Faults in the transmission or subtransmission system	$ \Delta V $, duration of event, possibly phase shift during event

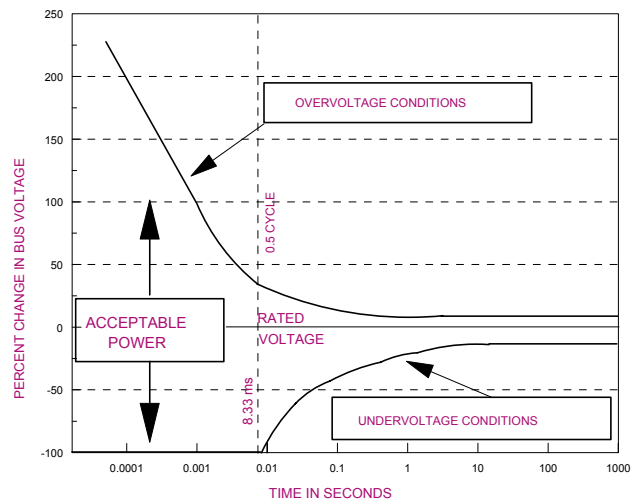


Fig. (1) The CBEMA power acceptability curve

References [1-3] discuss a fuzzy logic alternative to assess voltage - load sensitivity, testing of loads to CBEMA standards, and computer performance during voltage sags respectively. Bollen has discussed a classification system of voltage sags and their effects [4]. Ride through issues for adjustable speed drives appear in [5]. References [6] and [7] by Kyei and other researcher describe research into the 'derivation' of these curves by using data from appropriate models of loads.

It is evident that power acceptability curves have frailties in design and application. For example, very short duration events (e.g., less than a cycle in duration) have an ambiguity in the sense that the duration of the event may be difficult to identify, and the point-on-wave of the disturbance may have significant impact on the load. Point-on-wave information is not depicted in the $\Delta V-T$ plane. Further, the three phase implications of a power acceptability curve as indicated above are not clear: should one utilize phase information in the $\Delta V-T$ plane, or the positive sequence of the distribution voltage? Or is the graph basically a single phase representation? Another commonly asked question relates to the equation of the loci shown in Fig. (1). The CBEMA curve was developed from experimental and historical data: that is, cases of load disruption of mainframe computers were plotted in the $\Delta V-T$ plane, and a separator was developed to identify the acceptable and unacceptable regions.

II. A power quality standard

In 1998, Ayyanar and others [7] suggested the concept of a standard to represent whether power distributed is acceptable or unacceptable. The essence of the concept is that one needs to write a concrete criterion upon which acceptability is decided. One ultimate criterion of power acceptability relates to the operating status of the industrial process.

The particular power quality criterion depends on the nature of the load. For example, simple incandescent lighting loads may have a very loose criterion for acceptability, while certain sensitive computer controls may have a much more restrictive criterion. The difficulty in the selection of a single suitable criterion is confounded by the many possible load types. For simplicity, consider the rectifier load type depicted in Fig. (2). Voltage sags occur due to faults in the transmission, subtransmission, and primary distribution system, and they appear as low voltage conditions at V_{ac} depicted in Fig. (2). If the sag is of short duration and shallow depth, the ultimate industrial process 'rides through' the disturbance. This means that although V_{ac} is depressed, V_{dc} does not experience a sufficient disturbance to affect the load. The concept of a *voltage standard* is introduced at this point: a voltage standard is a criterion for power acceptability based on a minimum acceptable DC voltage at the output of a rectifier below which proper operation of the load is disrupted.

As an example of a voltage standard consider the following: if V_{dc} drops below 87% of rated voltage, the load is lost, and the distribution power is deemed to be unacceptable. The term 'standard' used in this context refers to the ultimate criterion upon which a decision of acceptability of supply is made. The use of the term 'standard' is not meant to imply an industry wide standard such as an IEEE standard. Fig. (3) shows a simulation study suitable for quantifying the effect of sags on rectifier load performance.

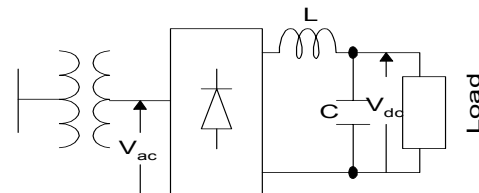


Fig. (2) A rectifier load

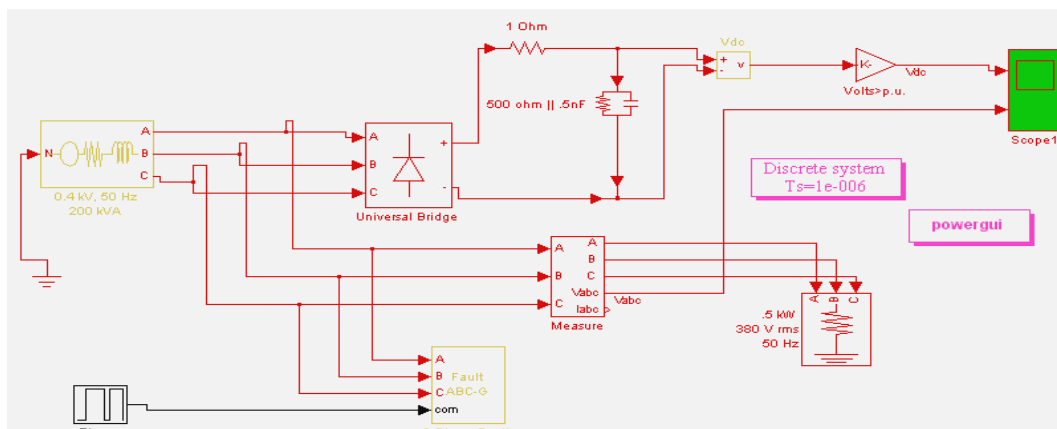


Fig. (3) Simulation of a three phase rectifier load

III. Analytical synthesis of the CBEMA curve

The CBEMA curve was derived from experimental and historical data taken from mainframe computers. The best engineering interpretation of the CBEMA curve can be given in terms of a voltage standard applied to the DC bus voltage of a rectifier load. Consider the case of either a single phase full wave bridge rectifier or the three phase bridge counterpart. Let the load on the DC side be an *RLC* load. If the DC bus voltage under a faulted condition is plotted as a function of the sag duration, the resulting curve is depicted in Fig. (4). From Fig. (4), the locus of V_{dc} could be represented as a double exponential in the form,

$$V_{dc}(t) = A + Be^{-bt} + C e^{-ct}.$$

Parameter A is the ultimate ($t \rightarrow \infty$) voltage, V_{end} , of the rectifier output. For the single phase case, and for the balanced three phase case, A is simply the depth of the AC bus voltage sag.

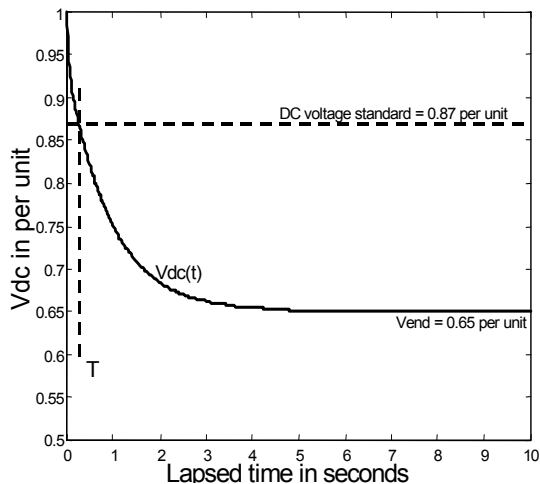


Fig. (4) Locus of $V_{dc}(t)$ under fault conditions (at $t = 0$) for a single phase bridge rectifier

For more complex cases, e.g. unbalanced sags, parameter A can similarly be identified as the ultimate DC circuit voltage if the sag were to persist indefinitely (this is readily calculable by steady state analysis of the given sag condition and the rectifier type). If three points are selected on the CBEMA curve to identify the *RLC* filter combination used in the rectifier types considered in the original CBEMA tests, one finds,

$$V_{dc}(t) = V_{end} + 0.288e^{-1.06t} + (0.712 - V_{end})e^{-23.7t}. \quad (1)$$

As an example, let the voltage standard be $V_{dc} \geq 0.87$. Then the V_{dc} excursion becomes unacceptable at T when $V_{dc} = 0.87$ in Equation (1). Solution for V_{end} in terms of $t = T$ in this expression gives

$$V_{end} = \frac{0.87 - 0.288 e^{-1.06T} - 0.712 e^{-23.7T}}{1 - e^{-23.7T}}.$$

This is the formula for the undervoltage limb of the CBEMA curve (V_{end} in per unit, T in seconds).

IV. Some practical considerations

Application of the CBEMA curve or most other power quality 'standards' require certain practical considerations. Among these non-ideal considerations are:

- The meaning of ΔV for short term events, especially when represented in root-mean-square (RMS) values
- Three phase considerations
- Non ideal sags (e.g., the sag is -10% for the first few cycles, followed by -15% for the next few cycles – or even less ideal conditions in which the sag has no well defined value
- Repeating events (e.g., one event, followed by restoration of normal operating conditions, followed by another event)
- Point-on wave issues (see Section 5)
- Multiple loads each with different sensitivity to bus voltage magnitude.

Some of these issues are more easily considered than others. However, the rectifier and $-87\% V_{dc}$ interpretation given above do apply in all the cited practical cases. That is, at least in theory, a given non ideal, and perhaps three phase case, could be simulated utilizing a rectifier load with a DC circuit filter of the type cited above in connection with the 'derivation of the CBEMA curve'. The three phase case is most easily considered as follows: Fig. (4) shows a power acceptability curve for a three phase rectifier. The case considered here is that of a phase A to ground fault using an $87\% V_{dc}$ voltage standard. The procedure for the development of the power acceptability curve is similar to the one employed in deriving Equation (1). The unbalanced rectifier is analyzed simply, and $V_{dc}(t)$ in this case is given as

$$V_{dc}(t) = V_{end} + 0.159e^{-0.158t} + (0.841 - V_{end})e^{-4.63t}. \quad (2)$$

In Equation (2), the time constants were obtained using an *LC* filter on the DC side of a three phase, six-pulse bridge rectifier. The values of the *LC* were chosen to agree with the filter design used in the single phase case mentioned in connection with the derivation of Equation (1). That is, the CBEMA curve was found to correspond to the single phase rectifier case plus filter *F*. If filter *F* is used as a filter in the *three phase* case, Equation (2) results. Select a voltage standard of $V_{dc} \geq 0.87$. When substituted into Equation (2) gives a formula for the power acceptability curve shown in Fig. (5) as

$$V_{end} = \frac{0.87 - 0.159 e^{-0.158 T} - 0.841 e^{-4.63 T}}{1 - e^{-4.63 T}}$$

Other unbalanced faults are analyzed similarly.

The issue of short term representation of ΔV in terms of RMS values was considered in [8]. In many power quality studies, waveforms are characterized through a RMS value,

$$F_{rms} = \sqrt{\frac{1}{T} \int_{t_0}^{t_0+T} f^2(t) dt}$$

where $f(t)$ is a time signal and T is either the period of the time signal or a suitably long time.

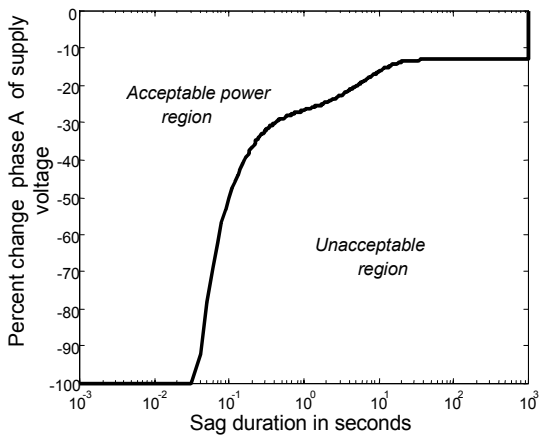


Fig. (5) Power acceptability curve for a three phase rectifier load with a phase-ground fault at phase A, 87% V_{dc} voltage standard

For the periodic case, when T is an integer multiple of the period of $f(t)$, and t_0 is a fixed point on the wave, the RMS value is termed a *synchronous RMS* (s-RMS). The s-RMS operation maps a time signal to a single point and can be visualized as an information concentrator. It is a simple matter to demonstrate that the s-RMS quantifies the Joule effect of a sinusoidal voltage or current. Reference [9] contains a discussion of applications and calculation procedures. Fig. (6) shows an example of a short term voltage sag for which the following key parameters are noted:

- T_w is the length of the observation time window
- T_s is the duration of the change in signal's amplitude
- T is the period of the signal, assumed as with sinusoidal variation
- T_0 is the moment of the amplitude change (considering that the observation window starts at $t = 0$)
- r is the magnitude of amplitude change (in p.u.; the reference value is the amplitude at $t < t_0$). Note that $r \leq 1$ and $r \geq 0$ for voltage sags, $r < 0$ for swells.
- ϕ is the phase at $t = 0$.

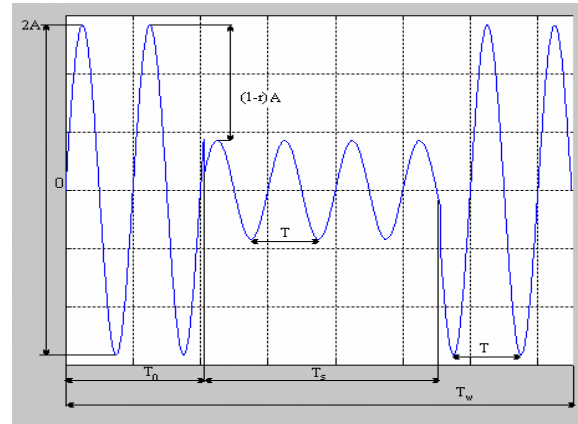


Fig. (6) Model of a voltage sag signal

In power quality studies, the effects on consumers are often quantified in terms of the deviation of secondary distribution voltage RMS values. However when sag events are of short duration, the RMS values may have a problematic interpretation.

There are many hardware and software algorithms which compute RMS values, and it becomes advisable to identify the hidden possible errors in calculation and interpretation. Note that the RMS operator is nonlinear, but working with F_{rms}^2 and $f^2(t)$ gives the linear formulation,

$$G_{rms} = F_{rms}^2 \quad g(t) = f^2(t) \quad G_{rms} = \frac{1}{T} \int_{t_0}^{t_0+T} g(t) dt. \quad \text{If}$$

the RMS operator is continuously carried out over a windowed time T , using past samples from the input signal $g(t)$, a moving average finite impulse response filtering is performed,

$$G_{rms T}(t) = \frac{1}{T} \int_{-\infty}^t g(\tau) r_T(\tau) d\tau$$

where $r_T(t)$ is a rectangular pulse which is zero everywhere except in the interval $[t-T, t]$ where it is unity. In the Fourier domain,

$$G_{rms T}(j\omega) = \frac{1}{j\omega T} G(j\omega) * R_T(j\omega).$$

The notation $(*)$ denotes frequency domain convolution. Equation (4) indicates that there is a frequency response interpretation to the RMS operator. References [10,11] further discuss factors relating to the calculation of the RMS value.

The problem of repeated events is considered in [12]. The concept of repeated events is problematic because a second event, following closely after a first event, could have greater impact than an isolated event that is identical to the cited second event. For example, a momentary sag occurring at $t = 0$, for six cycles, followed by a second event at $t = 0.15$ s (60 Hz system) of duration six cycles might be analyzed; in such a case, the analysis of the second event of six cycles is quite different from an analysis performed of an isolated, non-

repeated event of identical duration and sag depth. Heydt [12] suggests that there is a *recovery time* for which a system must progress in order to render an event in isolation from previous events. The concept of a recovery time is very similar to that of the ‘derivation of the CBEMA curve’ given above: that is, the recovery time of a sag can be plotted in the form of isopleths on a ΔV - T plane. The alternative, if the information is available, is to simulate the double (or triple, or multiple) event using a circuit as indicated in Figures (2) and (3).

The issues of multiple loads can be depicted as Fig. (7). For such a configuration, the CBEMA curve for each load may be calculated, tailoring the curve as needed. When the resultant CBEMA curves are drawn on a common ΔV - T plane, the inner area contains the acceptable region, and the outer area is the unacceptable region as shown in Fig. (8). The area(s) between the inner and outer regions represent power acceptable to some loads, and unacceptable to others.

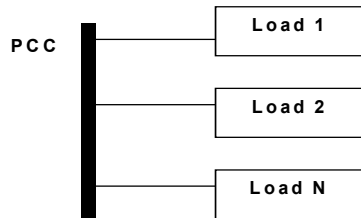


Fig. (7) Multiple loads at a point of common coupling (PCC)

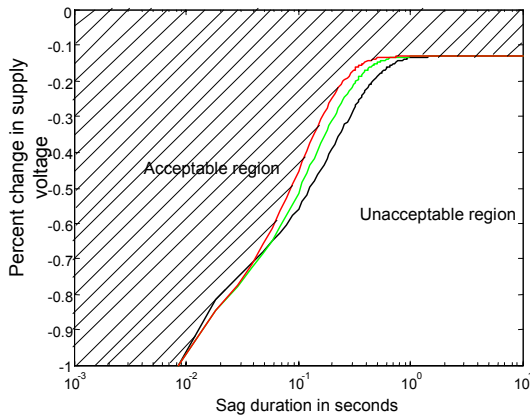


Fig. (8) Power acceptability region for the case of multiple loads

V. Point on wave issues

A momentary interruption of voltage or momentary sag in voltage magnitude may initiate at any point in the sinusoidal cycle as indicated in Fig. (9). For a linear load at unity power factor, the load current will be identical in phase to the indicated voltage. The energy transfer from the source to the load depends generally on θ_0 as well as the duration of the sag. Consider a total outage of supply voltage. Integrating $v(t)i(t)$ over θ_0 to $\theta_0 + \theta$ where θ is the duration of the sag represented in radians assuming 60 Hz (or 50 Hz as appropriate), one finds that the energy that should have been delivered during the sag (and is now unserved due to the outage) is W ,

$$W = \theta + \frac{\sin(\theta_0) - \sin(2\theta_0 + 2\theta)}{2} \quad (3)$$

For this simple formula, the rms supply voltage and current are both 1.0 per unit. Note that for values of θ that correspond to less than a half cycle (i.e., $\theta < \pi$), the CBEMA curve dictates that power delivery is ‘acceptable’. For longer duration outages, W depends not only on the duration of the outage θ , but also the point on wave θ_0 at the initiation of the sag.

The more general case of a linear load with power factor $\cos(\phi)$ is more involved since the instantaneous power is a double frequency sine wave whose DC offset (i.e., the average power) is proportional to $\cos(\phi)$. The unserved energy on total outage is

$$W = \theta \cos(\phi) - \cos(\phi) \frac{\sin(2\theta_0) - \sin(2\theta_0 + 2\theta)}{2} + \sin(\phi)(\cos(2\theta_0) - \cos(2\theta_0 + 2\theta)) \quad (4)$$

Collins and others have discussed the practical implications of the point on wave of the initiation of a voltage sag, including laboratory verified phenomena [13]. For long outages (large θ , e.g., much larger than three cycles or 6π radians), the term in Equations (3) and (4) that is proportional to θ dominates, and the unserved energy is no longer greatly dependent on the point on wave at the sag initiation.

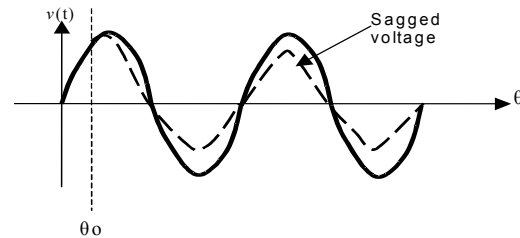


Fig. (9) Point on wave initiation of a voltage sag event

VI. A single index to show compliance with CBEMA

In most areas of engineering, it is important to use indices to measure or quantify the quality of performance. Power acceptability curves graphically depict power quality; but is there an index that can be used to assess ‘acceptability’ or ‘unacceptability’? Consider Fig. (10) in this matter. Point P represents an event $\Delta V = \Delta V_p$ and $T = T_p$ (shown as ‘unacceptable’ in Fig. (10)). As an index of power acceptability, it is proposed to vary the threshold V_T until the power acceptability curve passes through P . This is shown as dashed lines in Fig. (10). Then, one sets V_T to V_{Tp} ,

$$\Delta V_p = \frac{V_{Tp} + A(e^{-aT_p} - e^{-bT_p})}{1 - e^{-bT_p}} - 1$$

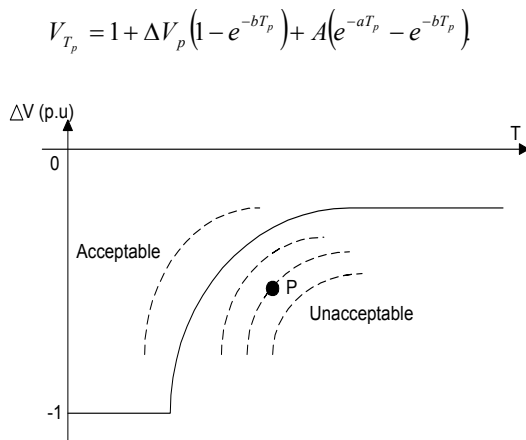


Fig. (10) Graphic interpretation of an index of power acceptability for an event P

Consider the index V_{T_p} / V_T . If $V_{T_p} / V_T \geq 1$, the point P represents an acceptable event. It is a simple matter to show that the theoretical maximum of the index V_{T_p} / V_T is $1/V_T$. Introduce the notation I_{pa} for the new index,

$$I_{pa} = V_{T_p} / V_T.$$

If one uses the notation T_x as the maximum time for which acceptable power is attained upon a total outage (i.e., $\Delta V = -1$),

$$I_{pa} = 1 + \Delta V_p \left(1 - e^{-bT_x}\right) + \frac{e^{-bT_x} - V_T}{e^{-bT_x} - e^{-aT_x}} \left(e^{-aT_p} - e^{-bT_p}\right)$$

This is an index of power acceptability for the event P . When the index is greater than unity, one is in the acceptable power region, and when the index is below unity, one is in the unacceptable region. At unity itself, the event is exactly on the CBEMA curve.

VII. Recommendations and concluding comments

In this paper, the CBEMA curve was revisited and the curve was analytically synthesized using a new concept, the voltage standard. The standard refers to an ultimate criterion that power is unacceptable if the DC voltage of a certain rectifier load drops below 87% of rated value. A double exponential equation describing the CBEMA curve is developed. This provides a useful method to consider the effect of unbalanced voltage sags and to develop CBEMA-like curves for other types of loads. A scalar index of compliance termed I_{pa} has been illustrated. This index is based on the CBEMA curve compliance.

Additional practical considerations relating to power acceptability include:

- The meaning of ΔV for short term events, especially when represented in root-mean-square (RMS) values

- Three phase considerations
- Non ideal sags
- Repeating events
- The energy served to a load during a sag as a function of the point-on-wave of the initiation of the event
- Multiple loads each with different sensitivity to bus voltage magnitude.

It appears that the main advantage of the CBEMA curve is the ease in application, and also in the familiarity of the concept by most power engineers. Although accuracy of the curve in predicting true acceptability – unacceptability of the power supply may not be a strong point of CBEMA technology, at least some problematic issues of its application may be resolved using the concept of a voltage standard.

Acknowledgements

The authors gratefully acknowledge the support of the Power Systems Engineering Research Center (PSerc) and SRP. Most of the work represented here came from Mr. John Kyei of the California ISO, Folsom CA. Dr. Raja Ayyanar of Arizona State University originated the concept of the voltage standard, and the authors acknowledge his contribution. Dr. Abu acknowledges the support of the Fullbright Fellowship.

References

- [1] B. Bonatto, T. Niimura, H. Dommel, "A fuzzy logic application to represent load sensitivity to voltage sags," Proceedings International Conference on Harmonics and Quality of Power, October, 1998, pp. 60-64.
- [2] E. Collins, R. Morgan, "A three phase sag generator for testing industrial equipment," IEEE Transactions on Power Delivery, v. 11, No. 1, January, 1996, pp. 526 - 532.
- [3] D. Koval, "Computer performance degradation due to their susceptibility to power supply disturbances," Conference Record, IEEE Industry Applications Society Annual Meeting, October, 1989, v. 2, pp. 1754 - 1760.
- [4] M. Bollen, L. Zhang, "Analysis of voltage tolerance of AC adjustable-speed drives for three-phase balanced and unbalanced sags," IEEE Transactions on Industry Applications, v. 36, No. 3, May-June 2000, pp. 904 -910.
- [5] E. Collins, A. Mansoor, "Effects of voltage sags on AC motor drives," Proceedings of the IEEE Technical Conference on the Textile, Fiber and Film Industry, 1997, pp. 9 - 16.
- [6] J. Kyei, "Analysis and design of power acceptability curves for industrial loads," MSEE Thesis, Arizona State University, Tempe AZ, December 2001.
- [7] J. Kyei, R. Ayyanar, G. Heydt, R. Thallam, J. Blevins, "The design of power acceptability curves," accepted for publication, IEEE Trans. on Power Delivery, 2003.

- [8] M. Albu, G. Heydt, "On the use of RMS values in power quality assessment," accepted for publication, IEEE Trans. on Power Delivery, 2003.
- [9] S. Kuo, B. Lee, Real-Time Digital Signal Processing. Implementations, Applications, and Experiments with the TMS320C55X, John Wiley and Sons, New York, 2001.
- [10] S. Herraiz-Jaramillo, G. Heydt, E. O'Neill-Carrillo, "Power quality indices for aperiodic voltages and currents," IEEE Transactions on Power Delivery, v. 15, No. 2, April 2000, pp. 784-790.
- [11] N. Tunaboylu, E. Collins, P. Chaney, "Voltage disturbance evaluation using the missing voltage technique," Proceedings of the 8th International Conference on Harmonics and Quality of Power 1998, pp. 577-582.
- [12] G. T. Heydt, Computer Analysis Methods for Power Systems, Second edition, Stars in a Circle Publications, Scottsdale, AZ, 1996.
- [13] E. R. Collins, M. A. Bridgwood, "The impact of power system disturbances on AC-coil contactors," Proceedings of the IEEE Technical Conference on the Textile, Fiber and Film Industry, 1997, pp. 2-6.